Dynamical history of the Local Group in ΛCDM – II. Including external perturbers in 3D

Article *in* Monthly Notices of the Royal Astronomical Society · January 2017

DOI: 10.1093/mnras/stx151

2 authors:

Indranil Banik
University of St Andrews
24 PUBLICATIONS **5** CITATIONS
SEE PROFILE

Hongsheng Zhao
University of St Andrews
168 PUBLICATIONS **4,491** CITATIONS
SEE PROFILE

MNRAS **000**, 1–19 (2016) Preprint 12 September 2016 Compiled using MNRAS LATEX style file v3.0

The High Velocity Galaxy Problem of ΛCDM in the Local Group – Including External Perturbers

Indranil Banik[1]*, Hongsheng Zhao[1]
[1]*Scottish Universities Physics Alliance, University of St Andrews, North Haugh, St Andrews, Fife, KY16 9SS, UK*

12 September 2016

ABSTRACT

We recently used an axisymmetric model of the Local Group (LG) to show that the observed positions and velocities of galaxies inside it are difficult to reconcile with the standard cosmological model, ΛCDM (MNRAS, 459, 2237). We now extend this investigation using a 3D model of the LG. This makes it feasible to directly include several other mass concentrations within and just outside the LG e.g. M33 and IC 342, respectively. As before, LG dwarf galaxies are treated as test particles.

Although our best-fitting 3D model yields different velocity predictions for individual galaxies, the overall picture remains unchanged. In particular, observed radial velocities (RVs) tend to exceed ΛCDM model predictions. The typical mismatch is slightly higher than in our earlier axisymmetric analysis, with a root mean square value of ~ 50 km/s. *Our main finding is that including the 3D distribution of massive perturbing dark matter halos is unlikely to help greatly with the high velocity galaxy problem.*

The anomalously high RVs of several LG dwarfs may be better explained if the Milky Way (MW) and Andromeda (M31) were once moving much faster than in our model. This would allow LG dwarfs to gain very high RVs via gravitational slingshot encounters with a massive fast-moving galaxy. Such a scenario is possible in some modified gravity theories, especially those which require the MW and M31 to have previously undergone a close flyby.

Key words: galaxies: groups: individual: Local Group – Galaxy: kinematics and dynamics – Dark Matter – methods: numerical – methods: data analysis – cosmology: cosmological parameters

1 INTRODUCTION

The dynamics of the Local Group (LG) of galaxies provided an early indication that our current understanding of physics is insufficient to explain the dynamics of astrophysical systems. Although the Universe must have started off expanding, the Andromeda (M31) and Milky Way (MW) galaxies are currently approaching each other at ∼110 km/s (Slipher 1913; Schmidt 1958). Their initial recession could not have been turned around in the ~ 14 Gyr (Planck Collaboration 2015) since the Big Bang if the luminous masses of these galaxies were attracting each other according to the inverse square law of Newtonian gravity.

The most commonly accepted solution is that most galaxies – including the MW and M31 – are surrounded by large amounts of dark matter (e.g. Ostriker & Peebles 1973). For a while, it was thought that this could be non-luminous conventional matter such as stellar remnants (e.g. Carr 1994, and references therein). However, gravitational microlensing searches for such massive compact halo objects indicated that there was not enough mass in them (Alcock et al. 2000; Tisserand et al. 2007). Thus, the required dark matter is thought to consist of an undiscovered stable particle, or at least one with a decay time longer than the age of the Universe (e.g. Steigman & Turner 1985, and references therein). Multi-decade searches for this particle have now ruled out a substantial part of the parameter space which was thought to be feasible before the searches started (e.g. Fermi-LAT Collaboration 2015; LUX Collaboration 2016).

Knowing only the separation and relative velocity of two galaxies, it would be very difficult to rule out this scenario. These two pieces of information are sufficient to constrain the relevant model parameters: the initial MW−M31 comoving separation and their total mass. Fortunately, much additional information has recently become available in the

*Email: ib45@st-andrews.ac.uk (Indranil Banik)
hz4@st-andrews.ac.uk (Hongsheng Zhao)

form of positions and velocities of many other LG galaxies (e.g. McConnachie 2012, and references therein).

The velocity field traced out by these galaxies should be understandable using the same MW and M31 total mass as is required to explain their present relative motion. An early attempt at such an analysis was made by Sandage (1986). There was some difficulty in matching all the data then available.

A more recent analysis based primarily on the catalogue of McConnachie (2012) also treated the gravitational field of the LG as spherically symmetric (Peñarrubia et al. 2014). Later, an adjustment was made for the effect of the Large Magellanic Cloud (LMC) on the MW, and thus on the observed velocities of all galaxies in the LG (Peñarrubia et al. 2016).

The MW and M31 can only be treated as a single point mass if their mutual separation d (783 ± 25 kpc, McConnachie 2012) is much less than the distance to the galaxy one is interested in. However, the LG only extends out to ~ 3 Mpc, making this assumption not very accurate within it. Further away, other massive objects besides the MW and M31 must also be considered.

Thus, we constructed an axisymmetric model of the LG in ΛCDM, which we consider reasonable because the low proper motion of M31 suggests an almost radial MW−M31 orbit (van der Marel et al. 2012a). A major nearby perturber to the LG is the Centaurus A group of galaxies (Harris et al. 2010). This lies very close to the MW−M31 line, allowing us to incorporate it into our model. Therefore, our simulation included 3 massive objects, with LG dwarfs treated as test particles. We previously published results based on this 2D model (Banik & Zhao 2016) and briefly review it here (Section 2).

Motivated by a poor match between the model and observations, we consider a 3D model of the LG (Section 3). The results obtained using it are described in Section 4. We go on to discuss how they compare with those obtained using our 2D model (Section 5). Here, we also consider a few factors beyond those included in our model. Section 5.1 is devoted to the effect of the Great Attractor on the LG. In Section 5.2, we consider the possible effects of a departure from the Newtonian gravity law assumed elsewhere in this work. Our conclusions are provided in Section 6.

2 REVIEW OF 2D AXISYMMETRIC MODEL

2.1 Governing Equations

We begin by reviewing our axisymmetric dynamical model of the LG (Banik & Zhao 2016), which in turn follows on from an earlier spherically symmetric analysis (Peñarrubia et al. 2014). Our simulations start at a redshift of 9, when the expansion of the Universe was nearly homogeneous (Planck Collaboration 2015). Thus, we assume that everything was following a smooth Hubble flow at that time. This means that the velocity $\boldsymbol{v}$ of each simulated particle would depend on its position $\boldsymbol{r}$ according to

$$\boldsymbol{v_i} \;=\; H_i \boldsymbol{r}_i \tag{1}$$

For any quantity k, we use k_i to denote its value at the time when our simulations are started and $\dot{k}$ to denote its time derivative. The expansion rate of the Universe is quantified by the Hubble parameter $H \equiv \frac{\dot{a}}{a}$, where a is the cosmic scale-factor. At the present time, $H = H_0$ and $a = 1$. In a flat Universe containing only matter and dark energy, their values at other times are given implicitly by

$$H\left(t\right) \;=\; H_0 \sqrt{\frac{\Omega_{m,0}}{a^3\left(t\right)} + \Omega_{\Lambda,0}} \tag{2}$$

We use a standard flat ($\Omega_{m,0} + \Omega_{\Lambda,0} \equiv 1$) dark energy-dominated cosmology whose parameters are given at the bottom of Table 2. Defining time t to start at the Big Bang ($a = 0$) and imposing the current expansion rate of the Universe as a boundary condition, we get that

$$a(t) \;=\; \left(\frac{\Omega_{m,0}}{\Omega_{\Lambda,0}}\right)^{\frac{1}{3}} \sinh^{\frac{2}{3}}\left(\frac{3}{2}\sqrt{\Omega_{\Lambda,0}} H_0 t\right) \tag{3}$$

LG dwarf galaxies are represented as test particles affected by the expansion of the Universe and by three massive particles − the MW, M31 and Centaurus A. The dynamics of test particles in such situations can be understood using General Relativity (Banik & Zhao 2016).

We constrain the massive particles to move along a line, making our model axisymmetric. Starting with a plane polar grid of initial positions, we advance the trajectories of a large number of test particles using the equation of motion

$$\ddot{\boldsymbol{r}} = \frac{\ddot{a}}{a}\boldsymbol{r} - \sum_{\substack{\text{j = MW,}\\ \text{M31, Cen A}}} \frac{GM_j\left(\boldsymbol{r} - \boldsymbol{r}_j\right)}{\left(|\boldsymbol{r} - \boldsymbol{r}_j|^2 + {r_{S,j}}^2\right)^{\frac{1}{2}} |\boldsymbol{r} - \boldsymbol{r}_j|^2} \tag{4}$$

r_S is chosen so that the force at $r \ll r_S$ leads to the correct flatline level of rotation curve for each galaxy, i.e. $r_S = \frac{GM}{{v_f}^2}$ where M is the mass of the relevant galaxy, whose rotation curve flatlines at the level v_f. For the MW, we take $v_f = 180$ km/s (Kafle et al. 2012) while for Andromeda, we use $v_f = 225$ km/s (Carignan et al. 2006). Because the separations between the massive galaxies are always quite large, for simplicity we use a pure inverse square law for the forces between them (i.e. r_S is set to 0 when calculating forces between the three massive particles). For test particles that get within ~ 15 kpc of a massive galaxy[1], we simply terminate the trajectory. It is likely that any real LG dwarf in this situation would be severely disrupted. Moreover, our analysis is concerned with LG dwarfs much further from any of the three massive galaxies in our model (Figure 1).

Our algorithm advances trajectories using a fourth order Runge-Kutta method based on an adaptive but quantised timestep, ensuring that the positions of the massive particles are available when needed. The timestep is adapted based on the distances between the object being advanced and the massive galaxies which influence its motion.

Our model is designed to accurately match the presently observed positions of galaxies within the LG as well as Centaurus A. Thus, we used a 2D Newton-Raphson algorithm to vary the initial relative positions of the MW, M31 and Cen A along a line in order to match their presently observed configuration to within an accuracy of $\sim 10^{-4}$. Solutions involving collisions between any of these galaxies were of course discarded. We were able to obtain a valid solution in

[1] 31 kpc for Cen A

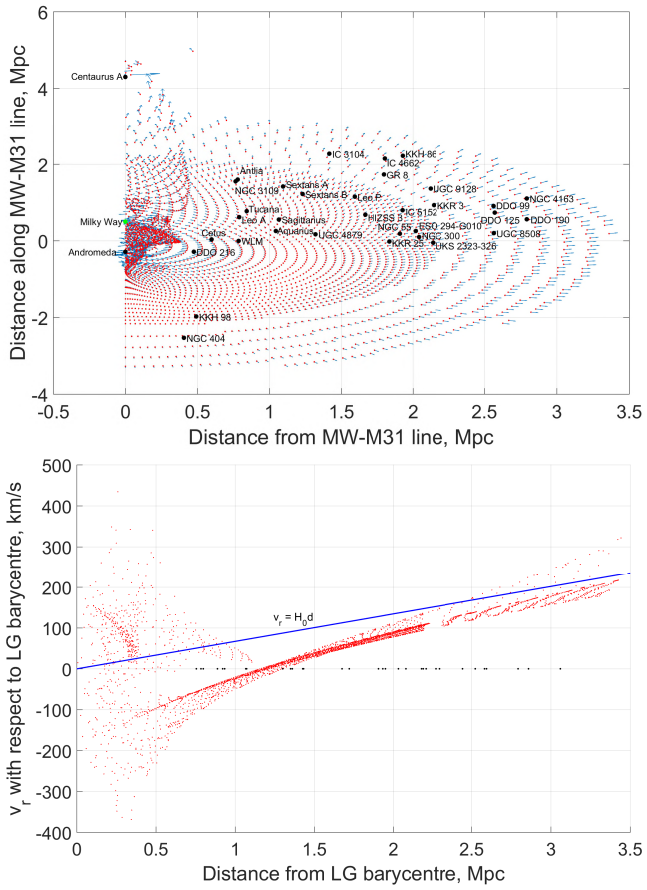

Figure 1. *Top:* Local Group velocity field for our best-fitting axisymmetric simulation (parameters given in Table 2). The radial resolution was degraded beyond a distance of 2.3 Mpc as the velocity field is generally quite smooth there. Locations of indicated galaxies are shown relative to the MW−M31 line. *Bottom:* Radial velocities of test particles with respect to the LG barycentre. Black dots on the x-axis show the distances of target galaxies from there. Without proper motions, observations can't be put on such a Hubble diagram because the MW is not at the LG barycentre.

all cases, though this was much easier if the algorithm was slightly under-relaxed for better stability.

Once the trajectories of the massive objects were known, we used Equation 4 to advance test particle trajectories. The resulting velocity field in one of our simulations is shown in Figure 1.

To get a test particle landing very close to the observed position of each LG dwarf galaxy, we could simply use a very dense grid of initial positions for our test particles. However, this would be very computationally intensive, especially if extended to 3 dimensions. Thus, we used a modest resolution grid and found which test particle landed closest to each target galaxy. We then used a 2D Newton-Raphson algorithm to vary the initial position of this test particle, targeting the desired final position. Because varying the trajectory of a test particle does not alter the gravitational field in the LG, we were able to improve the accuracy slightly, to $\sim 10^{-5}$.

The present velocity of the test particle on this trajectory is our model prediction for the velocity of the corresponding target galaxy. We subtract the simulated velocity of the MW and then project the relative velocity onto the direction towards the target to get its model-predicted Galactocentric Radial Velocity (GRV).[1]

The observational situation is complicated further by the motion of the Sun through the MW, $\boldsymbol{v}_\odot$. To convert observed heliocentric radial velocities (HRVs) into Galactocentric ones, we need an independent constraint on the motion of the Sun through the MW. Part of the challenge is determining $v_{c,\odot}$, the speed of a test particle on a circular orbit around the MW at the position of the Sun. This is called the Local Standard of Rest (LSR).

The other part is the non-circular component of $\boldsymbol{v}_\odot$, which consists of $U_\odot$ towards the Galactic Centre, $V_\odot$ in the direction of rotation and $W_\odot$ towards the North Galactic Pole. Our adopted values for these parameters are given in Table 2, the caption of which contains the relevant references. Given this information, we can determine actual GRVs using the relation

$$GRV_{obs} \;=\; HRV_{obs} + \boldsymbol{v}_\odot \cdot \widehat{\boldsymbol{d}_{MW}} \qquad (5)$$

Here, $\widehat{\boldsymbol{d}_{MW}}$ is the direction from the MW towards a target galaxy. The term $\left(\boldsymbol{v}_\odot \cdot \widehat{\boldsymbol{d}_{MW}}\right)$ represents a correction for Solar motion within the MW. Because $v_{c,\odot}$ is a model parameter, this correction is slightly model-dependent.

Instead of implementing the Solar motion correction via Equation 5, one could subtract it from the predicted GRV of a target galaxy to obtain its predicted HRV. Both procedures yield identical results because it is only the difference between model-predicted and observed GRVs which is relevant for our analysis (Section 2.2).

At large distances from the MW, it and M31 may be considered as a single point mass M. However, even in this case, the MW mass fraction $q_{MW} \equiv \frac{M_{MW}}{M}$ has a substantial effect on GRVs. This arises because smaller values of q_{MW} imply that the MW is moving faster with respect to the LG barycentre. As a result, even a spherically symmetric model of the LG can be used to place meaningful constraints on q_{MW}, as was recently done by Peñarrubia et al. (2014).

We have implicitly assumed that the motion of the Sun with respect to the disk of the MW is the same as its motion with respect to the MW barycentre, the important quantity for our analysis. This assumption may be invalidated if the MW has massive satellite galaxies. This does in fact seem to be the case, especially when considering the LMC (Peñarrubia et al. 2016).

In our models, the LMC is not treated as another particle but as a part of the MW. Thus, its simulated mass includes that of the LMC. Effectively, our model uses one particle to represent the MW system (≡ MW + satellite). This assumes that the LMC is bound to the MW, whose disk must then be moving with respect to the barycentre of the MW system due to the recoil induced by the LMC. Because it is very nearby compared to other LG galaxies of interest, we neglect the fact that observations made from

[1] Generally, LG galaxies are too far away to have accurate proper motions.

near the Sun are no longer made at the barycentre of the MW system.[1]

However, it is important to consider the motion of the LMC. Consequently, we determined $\boldsymbol{v}_{LMC}$, its space velocity with respect to the MW. This requires knowledge of its HRV (McConnachie 2012) and its proper motion (Kallivayalil et al. 2013) multiplied by its distance (Pietrzyński et al. 2013). This information was used to obtain a revised estimate for the motion of the Sun with respect to the MW system

$$\boldsymbol{v}_\odot \rightarrow \boldsymbol{v}_\odot - q_{LMC}\boldsymbol{v}_{LMC} \quad (6)$$

$$q_{LMC} \equiv \frac{M_{LMC}}{M_{MW}} \quad \text{(MW includes LMC)} \quad (7)$$

Although M31 may have massive satellites too, we do not consider them because they do not affect our analysis to the same extent. A massive satellite of M31 can create a mismatch between the present GRV of the M31 disk and that of the M31 system. However, this does not affect the GRV of any other target galaxy. Because M31 is only one of our 34 target galaxies, our analysis should not be much affected by a slight problem with its GRV. This is not true if the MW had a massive satellite as that would affect our velocity relative to everything else.

2.2 Statistical analysis

We used our axisymmetric model to predict GRVs of target galaxies where it was possible to obtain a unique prediction. This is not always the case, as is clear from Figure 1. In the region between the MW and M31, intersecting trajectories are apparent. This means that there is more than one possible velocity at the same position, even within the same model. Thus, we do not have any targets within this region. Based on this consideration, we made some adjustments to the catalogue of galaxies used by Peñarrubia et al. (2014) for our analysis in Banik & Zhao (2016).[2]

To handle distance uncertainties, we recalculated GRV predictions with each target galaxy moved along the line of sight to the 1σ upper limit of its observed distance d_{MW} (using the 1σ lower limit instead yielded almost identical results).

$$\sigma_{pos} \equiv |GRV_{model}\left(d_{MW}+\sigma_{d_{MW}}\right) - GRV_{model}\left(d_{MW}\right)| \quad (8)$$

Here, $\sigma_{d_{MW}}$ is the uncertainty in the distance to a target galaxy whose most likely distance is d_{MW}. Position uncertainties are effectively along a line because sky positions are known very accurately, even if distances are not. Assuming the velocity field in the LG is roughly linear over the part of this line where the target might actually be and that distance errors are Gaussian, the model-predicted GRV also has a Gaussian distribution. This allows us to straightforwardly combine HRV measurement uncertainties σ_{v_h} with those on GRV predictions caused by distance uncertainties. Thus, the contribution to the χ^2 statistic from any galaxy i is

$${\chi_i}^2 \equiv \left(\frac{GRV_{model}-GRV_{obs}}{\sigma}\right)^2 \quad \text{where} \quad (9)$$

$$\sigma = \sqrt{{\sigma_{pos}}^2+{\sigma_{v_h}}^2} \quad (10)$$

Uncertainty in the distance to M31 has other subtle effects on our analysis. The gravitational field in the LG would be altered if M31 was at a different distance than the assumed 783 kpc. However, we neglect such effects because, towards the edge of the LG, the only relevant factors are the masses of the MW and M31.

Although we use uniform priors on most model parameters, this is not true with the LSR speed $v_{c,\odot}$. For this, we assume a Gaussian prior of 239 ± 5 km/s (McMillan 2011) and add a corresponding contribution to the total χ^2. Thus,

$$\chi^2 = \left(\frac{v_{c,\odot}-v_{c,\odot,\text{nominal}}}{\sigma_{v_{c,\odot}}}\right)^2 + \sum_{\substack{\text{Target}\\ \text{galaxies}}} {\chi_i}^2 \quad (11)$$

Because σ_{pos} varies slightly with model parameters, our error budgets become model-dependent. Thus, the best-fitting model is not just that which minimises χ^2. We quantify the relative probabilities of different models using

$$P(\text{Model} \mid \text{Observations}) \propto \mathrm{e}^{-\frac{\chi^2}{2}} \prod_i \frac{1}{\sigma_i} \quad (12)$$

We will focus on how observed GRVs deviate from those predicted by our best-fitting model. To facilitate the discussion, we define

$$\Delta GRV \equiv GRV_{obs} - GRV_{model} \quad (13)$$

2.3 2D Results

In Figure 2, we compare model-predicted and observed GRVs in the best-fitting model (parameters given in third column of Table 2). We also show results for Cetus and DDO 216. Despite being quite close to M31, they seem to be in a region with a smooth velocity field (Figure 1). This allows for a well-defined model prediction. However, the absence of M33 from our model may make these predictions less reliable than for other target galaxies. This is especially true with DDO 216, which is closer to M31. We will return to this point later.

There is a tendency for observed GRVs to exceed model predictions (Figure 2). To gain a better feel for this phenomenon, we constructed a histogram of all the ΔGRVs. Errors due to distance and HRV uncertainties are accounted for by convolving each data point with a Gaussian of the appropriate width (Equation 10). To account for an uncertain LSR speed (which is only weakly constrained by our investigation), we also added the 5 km/s uncertainty on this in quadrature. The results are shown in Figure 3.

Our model is not a perfect representation of ΛCDM and can only really be expected to get GRV predictions accurate to $\sim$25 km/s (Aragon-Calvo et al. 2011). Thus, one expects the distribution of ΔGRVs to be broadly consistent with a Gaussian of this width. Indeed, this appears to be the case for those galaxies with $\Delta GRV < 0$ (highlighted blue in Figure 3 as they appear blueshifted relative to our model).

[1] We also take the Sun to be the centre of the MW disk. However, a fixed distance of 8 kpc is used in our 3D model (Section 3).
[2] Andromeda XVIII was excluded and HIZSS 3 A & B were assumed bound, with a mass ratio of 13:1 (Begum et al. 2005).

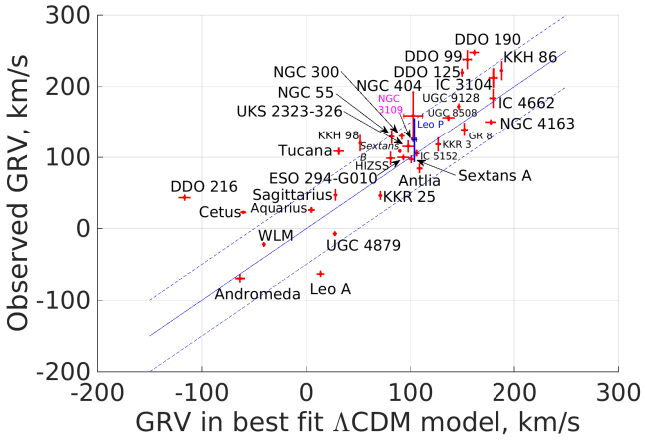

Figure 2. Comparison between predicted and observed GRVs of indicated galaxies in our best-fitting axisymmetric model including Centaurus A and the LMC. The adopted model parameters are given in Table 2. The line of equality is shown in solid blue. Two parallel lines (dashed blue) offset by 50 km/s are also shown. Assuming our model is accurate to $\sim$25 km/s, it is unlikely in the context of ΛCDM to find many galaxies far outside this range. Generally, a larger GRV indicates a larger distance (for reference, Aquarius is $\sim$1 Mpc from the LG barycentre).

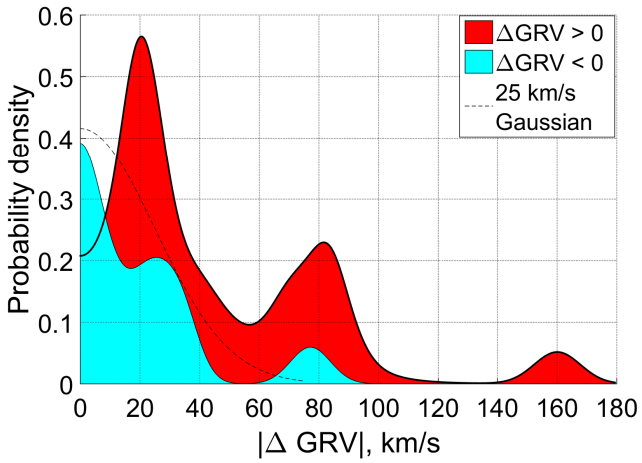

Figure 3. Histogram showing observed − predicted GRVs of our target galaxies using our best fitting 2D model. The area of each square corresponds to 2 galaxies. Each data point was convolved with a Gaussian of width $\sigma = \sqrt{{\sigma_{pos}}^2 + {\sigma_{v_h}}^2 + {\sigma_{v_{c,\odot}}}^2}$. We divided our sample into those with $\Delta GRV < 0$ (blue) and those with $\Delta GRV > 0$ (red). A Gaussian of width 25 km/s is overplotted as a short-dashed line. This matches the $\Delta GRV < 0$ subsample quite well, especially when Leo A is excluded as this removes the blue bump near 75 km/s.

On the other hand, this is not true for galaxies which have $\Delta GRV > 0$. One can dismiss the bump in the histogram near 160 km/s due to DDO 216 on the grounds that it may be too close to M31 and thus the velocity field may be disturbed there. This is not the case in our model (Figure 1) but one can envisage that it is true in the real world when one considers additional effects e.g. interactions with massive M31 satellites such as M33. However, it is very difficult to dismiss the bump at 80 km/s in this way because it corresponds to several galaxies, some of which are quite far from the LG (top panel of Figure 13). The presence of this feature along with the expected bump near $\Delta GRV = 0$ suggests the existence of some additional process responsible for a few galaxies having GRVs much higher than expected in our model. We consider some possible solutions to this high velocity galaxy problem in Section 5.

At the positions of our target galaxies, we expect the velocity field of the LG to be smooth (Figure 1). To see if this is the case, we determined the distance between each pair of targets and the difference in their ΔGRVs (Figure 4).[1]

Our prediction of a smooth velocity field relates to the centres of mass of field halos in a more detailed cosmological N-body simulation. However, the situation is different for individual simulation particles. Their velocity dispersion inside each halo prevents a unique velocity prediction based on position only. This arises because individual simulation particles do not correspond to the observed kinematics of LG dwarfs. Consequently, care is required if comparing our results with cosmological simulations.

Some examples are apparent where galaxies are quite near each other but have a very different ΔGRV. In these situations, because model predictions should be very similar, the difference in ΔGRVs must be mostly due to a difference in observed HRVs. More information is given about some of these cases in Table 1.

A few such discrepant pairs are expected given that there are 561 pairs in total. However, the magnitude of the difference between ΔGRVs is rather large in some cases, suggesting that the velocity field in the LG may not be as smooth as in our model. The most convincing examples of this are related to the galaxy NGC 4163, without which the case for a disturbed velocity field is greatly weakened. The galaxies near it (DDO 99, 125 and 190) all seem to have much higher ΔGRVs, suggesting that perhaps the GRV of NGC 4163 is unusually low. In fact, it has the third-lowest ΔGRV of -26.9 ± 7.6 km/s. This may not seem like much, but we will see later that a more detailed 3D model of the LG predicts a much higher GRV for this galaxy than is observed (Section 3).

Previously, we considered a number of possible explanations for the high velocity galaxy problem but concluded that none of them were likely to resolve it (Banik & Zhao 2016, Section 4). For example, we altered the start time of our simulations to correspond to when $a = \frac{1}{15}$ instead of $\frac{1}{10}$ (see their Section 4.6). This reduced the root mean square (rms) value of ΔGRV, but only by $\sim$1 km/s. The small effect is an unavoidable consequence of Hubble drag, which causes present deviations from the Hubble flow to be fairly insensitive to the forces acting at early times.

As our model does not include several galaxy groups only a little outside the LG, we constructed a basic model to estimate their effects. Tides are more important for target galaxies further away from us, so we simplified our model to treat the MW and M31 as only one object. The perturber was treated as a second massive object, with the

[1] Errors on mutual separations are over-estimated because we add distance errors in quadrature.

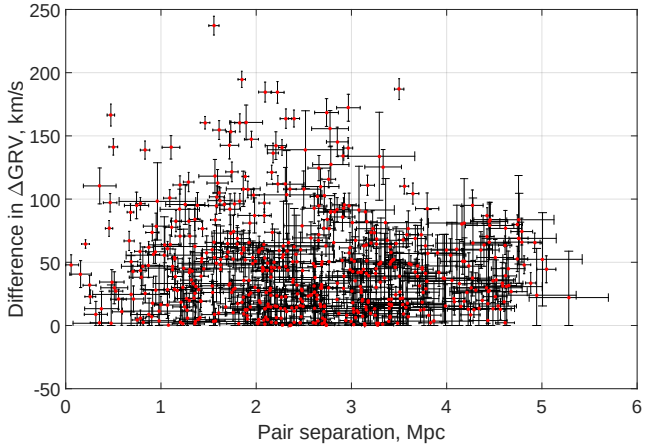

Figure 4. Distances between galaxies in our sample are shown here against the difference between their ΔGRVs. The errors on these correspond to errors on measured distances and radial velocities of both galaxies being compared. For galaxies near each other, model predictions for their GRVs will be similar such that the y-axis essentially just shows the difference between their observed HRVs. Sometimes, these differences are large even for nearby galaxies. These cases appear towards the upper left potion of this figure and some of them are listed in Table 1.

Galaxy 1	Galaxy 2	Separation (Mpc)	Ratio	Difference in ΔHRV (km/s)
DDO 99	NGC 4163	0.36±0.17	0.13±0.06	110.4±14
DDO 125	NGC 4163	0.47±0.07	0.17±0.03	97.1±7.3
KKR 3	DDO 190	0.74±0.13	0.30±0.05	95.0±10.5
Andromeda	DDO 216	0.47±0.04	0.56±0.05	166.5±8.6
WLM	DDO 216	0.50±0.05	0.54±0.05	141.3±6.5
UGC 8508	DDO 190	0.67±0.05	0.25±0.02	66.9±7.6
WLM	Cetus	0.21±0.04	0.25±0.05	64.5±3.4

Table 1. Differences between the ΔGRV of nearby galaxies are shown here, with our 2D model used to obtain predicted GRVs. The error budgets account for uncertainties in HRV and distance measurements of both targets. Their separation is shown in physical units and as a fraction of the mean of the distances from the MW to each of them. We show only the most extreme examples of galaxies near each other but with a very different ΔGRV (most convincing examples near top). Results for all galaxy pairs are shown in Figure 4.

target modelled as a test particle at the appropriate position. We obtained a test particle trajectory satisfying Equation 1 initially and reaching this position at the present time. We then found its radial velocity with respect to the LG particle. Our estimate for the effect of the perturber on the GRV of the target was found by repeating this calculation with the perturber mass reduced to zero. These estimates suggested that IC 342 and M81 would make it even more difficult to explain the observed GRVs of the most discrepant objects (Banik & Zhao 2016, Table 6).

A 3D model allows us to test these conclusions more rigorously by directly including many more objects, several of which are quite far from the MW−M31 line. The inclusion of the LMC and M33 can help to make our model more reliable closer to the MW and M31, respectively. This is one reason why we felt comfortable adding Cetus and DDO 216 to our sample. Our model should also be more reliable further from the LG as it now includes more of the most massive objects just outside it. However, we do not take advantage of this by expanding our sample outwards.

Parameter	Meaning & units	Best-fitting value in 2D	Best-fitting value in 3D
M	LG mass, $10^{12}M_\odot$	2.756	4.088
q_{MW}	$\frac{M_{MW}}{M}$	0.356	0.497
q_{LMC}	$\frac{M_{LMC}}{M_{MW}}$	0.157	0.099
$v_{c,\odot}$	LSR speed, km/s	239	223.0
$v_{f,M31}$	v_f of M31, km/s	225	240.3
d_{M31}	Distance to M31, kpc	783	707
$M_{\text{Cen A}}$	Cen A mass, $10^{12}M_\odot$	4	5.883
$U_\odot$	Components of the	14.1	11.1
$V_\odot$	non-circular motion of	14.6	12.2
$W_\odot$	Sun in the MW, km/s	6.9	7.2
H_0	Hubble constant	67.3	70
$\Omega_{m,0}$	Present matter density in the Universe $\div \frac{3{H_0}^2}{8\pi G}$	0.315	0.27

Table 2. The parameters of our best-fitting axisymmetric (2D) and 3D models are given here. q_{LMC} is defined in Equation 7, where the LMC is taken as part of the MW. The fraction of the MW+M31 mass M in the MW is q_{MW}. The top section of this table contains the parameters we varied using a grid search in our 2D model (Banik & Zhao 2016) or using a gradient descent method in 3D (Section 3.2). The central section contains the parameters associated with the non-circular motion of the Sun in the Milky Way (Francis & Anderson 2014) and two parameters related to M31. In the 2D model, its distance estimate is from McConnachie (2012) while the 3D model uses a prior of 770 ± 40 kpc (Ma et al. 2010). Its rotation curve flatlines at a level $v_{f,M31}$ which is fixed in the 2D model but has a prior of 240 ± 10 km/s in the 3D model (Carignan et al. 2006). This model assumes $v_f = v_{c,\odot}$ for the MW whereas the 2D model fixes the former at 180 km/s (Kafle et al. 2012) and uses a prior on the latter of 239 ± 5 km/s (McMillan 2011). We adopt a flat dark energy-dominated cosmology whose parameters are fixed at values given in the bottom section (Planck Collaboration 2015). Both models start when the cosmic scale-factor $a = 0.1$.

3 THE 3D METHOD

3.1 Governing equations

The 3D algorithm we employ is explained in more detail in Appendix A of Peebles et al. (2011), which applies the numerical action method to solve the governing equations. A more detailed attempt was later made to use this method to understand the dynamics of LG galaxies (Peebles & Tully 2013). We briefly review some of the key aspects of how the model works.

The equation of motion for test particles is

$$\ddot{\boldsymbol{r}} = {H_0}^2 \Omega_{\Lambda,0} \boldsymbol{r} - \sum_{\substack{\text{j = Distant} \\ \text{massive} \\ \text{particles}}} \frac{GM_j \left(\boldsymbol{r} - \boldsymbol{r}_j\right)}{|\boldsymbol{r} - \boldsymbol{r}_j|^3} - \sum_{\substack{\text{j = Nearby} \\ \text{massive} \\ \text{particles}}} \frac{GM_j \left(\boldsymbol{r} - \boldsymbol{r}_j\right) \left({r_c}^2 + {r_{S,j}}^2\right)}{\left(|\boldsymbol{r} - \boldsymbol{r}_j|^2 + {r_c}^2\right) {r_{S,j}}^3} \tag{14}$$

For massive particles, the value of r_S used corresponds to the galaxy with the larger r_S. The massive objects included in our analysis are listed in Table 3. The distances and HRVs shown are best-fitting values obtained based on trying to match all observational constraints within their uncertainties (Section 3.2).

Some differences with Equation 4 are apparent. The part of the cosmological acceleration $\ddot{a}$ caused by dark energy is handled in the same way but the part caused by matter is not. Previously, we treated the Universe as homogeneous except for a few massive particles. This meant that, without these particles, we would need to recover the cosmic expansion $\boldsymbol{r} \propto a$, which is only possible if $\ddot{\boldsymbol{r}} = \frac{\ddot{a}}{a}\boldsymbol{r}$.

Here, we treat the Universe as empty except for the massive particles that we explicitly include. Because the Universe is homogeneous on large scales, an accurate understanding of all the mass interior to a sufficiently distant test particle also leads to its separation from us changing with time as $\boldsymbol{r} \propto a$.

The gravitational field near massive particles is handled slightly differently here. An explicit distinction is now drawn between massive particles within r_S of any given test particle and masses further away, forces from which are handled using a pure inverse square law. Forces from nearby masses at first rise linearly with separation before falling as $F \propto \frac{1}{r}$, recovering the observed flat rotation curves of galaxies. The transition occurs around a radius of r_c, which is fixed at 10 kpc.

For the MW and M31, we define r_S in the same way as previously, though we now add the assumption that the LSR speed is the same as v_f for the MW. Its value is allowed to float, with a prior assumption of 240 ± 10 km/s. We use the same value for M31. For other massive galaxies, we assume $r_S = 100$ kpc to avoid an adjustment each time their masses are altered.

The equations of motion are solved by adjusting a trial trajectory towards the true one. An incorrect trajectory will have a mismatch between the acceleration along it and that expected due to the gravity of other particles. Thus, at each timestep, the positions of all the particles are adjusted to try and equalise the gravitational field acting on each one with the acceleration $\ddot{\boldsymbol{r}}$ it experiences along its trajectory. This is done assuming both respond linearly to a position adjustment, although only the latter does. Thus, a solution can only be obtained after several iterations, each of which is reliant on a matrix inversion to handle the highly inter-connected nature of the problem. Certain shortcuts are taken for test particles because their position has no effect on the forces felt by other particles.

This method of solution is second-order accurate because of the standard finite differencing scheme used to obtain accelerations from a series of discrete positions valid at known times. Due to the large number of particle pairs, an adaptive timestep scheme is impractical. Instead, we adapt the temporal resolution to the problem in a fixed way based on physical considerations. Each timestep corresponds to an equal increment in the cosmic scale-factor a. We use 500 steps between when $a = 0.1$ and the present time ($a \equiv 1$).

To check if we have adequate resolution, the problem is solved using forward integration instead with 5000 timesteps equally spaced in a. The maximum error in the present position is 0.23 kpc while that in the velocity is 0.84 km/s. Both these numbers are very small, suggesting that we have enough resolution. Some other checks are also done to verify the numerical accuracy of our solution (Peebles et al. 2011, Section 2.4).

The Hubble diagram for our best-fitting 3D model is shown in Figure 5. For comparison, we overlay results from an axisymmetric model using the same model parameters (last column of Table 2). The basic trend of increasing radial velocity with distance is apparent in both models.

Galaxy	Distance, Mpc	HRV, km/s	Mass, $10^{12} M_\odot$
Milky Way	0.008	−11.10	1.8302
Andromeda (Messier 31)	0.707	−309.18	2.0567
Centaurus A	3.736	504.52	5.8831
Messier 101	7.391	439.62	9.3108
Messier 94	4.366	324.31	8.8144
Sculptor	4.095	246.97	6.9296
NGC 6946	5.859	107.38	4.6142
Messier 81	3.625	73.48	4.0625
Maffei	3.988	−28.75	3.4924
IC 342	3.350	−12.98	1.2994
Triangulum (Messier 33)	0.948	−192.72	0.2214
Large Magellanic Cloud	0.065	235.97	0.2007
NGC 55	2.035	163.16	0.1323
NGC 300	1.963	158.70	0.1073
IC 10	0.781	-338.02	0.0437
NGC 185	0.706	−213.37	0.0129
IC 5152	1.878	138.56	0.0094
NGC 147	0.679	−201.04	0.0064
NGC 6822	0.510	−69.93	0.0059

Table 3. Data on the massive galaxies in our 3D model. Distances are allowed to vary slightly to best match observations. The top section contains galaxies which are also directly included in our 2D model. The remaining galaxies are sorted in descending order of simulated mass. For clarity, we abbreviated the names of galaxies from the New General Catalogue (NGC) and Index Catalogue (IC).

3.2 Statistical analysis

Like our axisymmetric model, our 3D model accurately matches the observed sky positions of target galaxies because it integrates the equations of motion backwards from the present time. However, we no longer require agreement between simulated and observed heliocentric distances. Instead, we add a contribution to the total χ^2 of the model if there is a mismatch. This means that error budgets are no

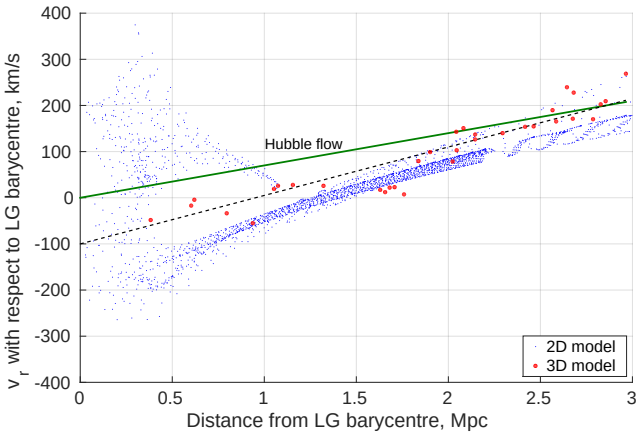

Figure 5. Radial velocities of test particles with respect to the LG barycentre are shown in blue for our 2D model with parameters matched to our best-fitting 3D model (Table 2), results of which are shown as large red dots. The solid green line is the Hubble flow relation for $H_0 = 70$ km/s/Mpc, our adopted value. The dashed black line has a gradient 1.5× larger. Due to the effect of gravity, it provides a better fit to the 3D model within the LG.

longer model-dependent, making the determination of relative model likelihoods equivalent to a simple comparison of their χ^2 statistics.

The distance errors σ_d come from observations. For M31, we use a slightly closer and more uncertain estimate (770 ± 40 kpc, Ma et al. 2010). Galaxies outside the LG might be affected by objects beyond the region covered by our analysis. It can also be difficult to determine the mass ratios between galaxies in an extended group and thus the location of its centre of mass. For these reasons, we use a fairly large uncertainty for such distant objects.

$$\frac{\sigma_d}{d_{MW}} = \frac{1}{10} \quad \text{if } d_{MW} > 3.2 \text{ Mpc} \tag{15}$$

Mismatches between observed and simulated GRVs are handled similarly, based on a tolerance of 20 km/s rather than the actual HRV measurement uncertainty. This is because we do not expect our model to be much more accurate as a representation of ΛCDM considering the level of scatter about the Hubble flow in more detailed simulations (Aragon-Calvo et al. 2011). As σ_{v_h} is always much smaller than this, the effect of raising it to 20 km/s is similar to adding an extra 20 km/s dispersion term to Equation 10. This prevents the model placing undue statistical weight on a galaxy with very precise observations, given that the model itself also has uncertainties.

We made use of proper motion data for M31, M33, the LMC, IC10 and Leo I. This was done by adding a penalty to χ^2 when simulated and observed values disagree, with observational error estimates taken at face value.

Unlike in our 2D model, Equation 1 is no longer strictly enforced at the start of our simulations because this is difficult to achieve when integrating backwards. Instead, we penalise models which fail to enforce it.

$$\Delta\chi^2 = \frac{|\overbrace{\boldsymbol{v}_i - H_i \boldsymbol{r}_i}^{\boldsymbol{v}_{pec}(t=t_i)}|^2}{{\sigma_v}^2} \tag{16}$$

We assume that the typical peculiar velocity $\boldsymbol{v}_{pec}$ when $a = 0.1$ was $\sigma_v = 50$ km/s based on typical present-day deviations from the Hubble flow (Figure 5). This is a 1D measure which underestimates typical values of v_{pec} today. However, the nearly homogeneous state of the Universe at recombination (Planck Collaboration 2015) implies v_{pec} was typically smaller when our simulations started than it is today. The distribution of v_{pec} at that time is shown in Figure 6 for our best-fitting 3D model. All 50 galaxies in this model are represented, some of which are outside the LG (Table 3).

We now allow some of our target galaxies to have mass, even if they were treated as test particles previously. This change applies to IC 4662, IC 5152, NGC 55 and NGC 300. Naturally, we do not fix the masses of any of our simulated galaxies which have any. However, the prior we use is non-uniform and prefers a particular value. This is based on assuming a mass to light ratio of 50 times the Solar value in the near-infrared K-band (Tully et al. 2013).

Observational estimates of the luminosity in this band L_K are based on assuming a particular distance to each target. If e.g. the distance in the model is less, then the model implies that the target is likely closer to us and thus intrinsically fainter for the same apparent magnitude. This makes it likely to be less massive. Accounting for this, we define the preferred mass estimate

$$M_c \equiv 50 L_K \left(\frac{M}{L_K}\right)_\odot \left(\frac{d_{model}}{d_{obs}}\right)^2 \tag{17}$$

Using a different mass M incurs an extra χ^2 cost of

$$\Delta\chi^2 = \left[\frac{Ln\left(\frac{M}{M_c}\right)}{Ln\ 1.5}\right]^2 \tag{18}$$

For the MW and M31, a slightly different procedure is used. There is no a priori preference towards any particular mass for either galaxy, but a particular *ratio* between their masses is preferred. This is the ratio of their values of M_c.

$$\Delta\chi^2 = \tag{19}$$

$$\left[\frac{(Ln\ M_{MW} - Ln\ M_{M31}) - (Ln\ M_{MW,c} - Ln\ M_{M31,c})}{Ln\ 1.25}\right]^2$$

Our model now has too many parameters to permit a grid search through them. Thus, we only present results from our best-fitting 3D model. This is obtained by minimising χ^2. The minimisation procedure involves a downhill-seeking walk through parameter space (Peebles et al. 2011, Section 2.2). Each parameter A is varied by a small amount δA in an attempt to reduce χ^2. If this does not happen, then the algorithm restores the previous solution and sets

$$\delta A \rightarrow -\frac{1}{2}\delta A \quad (\chi^2 \text{ increased}) \tag{20}$$

As well as reversing the sign of δA, it is important to reduce its magnitude because the increase in χ^2 is often caused by overshooting its minimum with respect to A.

When we are fortunate in that a parameter adjustment reduces χ^2, we accelerate the convergence by setting

$$\delta A \rightarrow \frac{5}{4}\delta A \quad (\chi^2 \text{ decreased}) \tag{21}$$

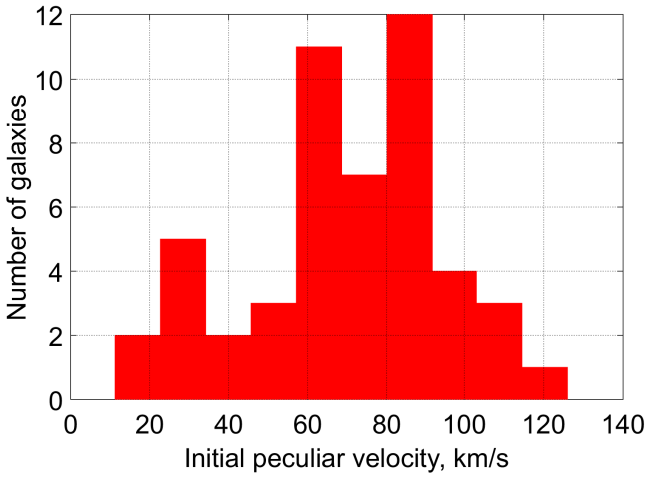

Figure 6. Histogram showing deviations from the Hubble flow (Equation 1) at the start of our best-fitting 3D simulation. We allow a tolerance of 50 km/s (Equation 16). The mean result is 69 km/s, with a 1σ confidence interval of 38−91 km/s.

To avoid the parameter adjustments being too small or too large, a cap and floor are imposed on $|\delta A|$ such that

$$10^{-5} \; < \; \left|\frac{\delta A}{A}\right| \; < \; 10^{-1} \qquad (22)$$

4 3D RESULTS

We started with a solution to the equations of motion which best matched available constraints on the massive galaxies in our analysis (Table 3). We then added test particles one at a time, giving the algorithm an opportunity to adjust the trajectories of the massive objects in order to better accommodate observational constraints from the corresponding LG dwarf. After adding our complete sample, we varied all the parameters one at a time to see if we could achieve any further reduction in χ^2. After repeating this a few times, it became clear that the preferred solution was not changing. Some of the most important parameters associated with this model are shown in Table 2.

The optimal value of q_{MW} is 0.50, slightly higher than the 0.36 ± 0.04 preferred by our axisymmetric analysis (error budgets estimated from Banik & Zhao 2016, Figure 18). This is because our 3D model puts M31 at a distance of only 707 kpc (Table 3), much less than the most likely distance of 783 kpc (McConnachie 2012). If the model is to be trusted, then the known apparent magnitude of M31 combined with a closer distance implies that it is intrinsically fainter. This reduces the preferred mass of M31 (Equation 17). If we scale up the mass of M31 by $\left(\frac{783}{707}\right)^2$, then q_{MW} would fall to 0.45. Treating M33 as part of M31 raises its mass, reducing q_{MW} a further ~ 0.03. This makes it consistent with our axisymmetric analysis, assuming both yield similarly uncertain estimates of q_1.

We consider several galaxies close enough to M31 for the flatline level of its rotation curve to make a difference. This is especially true with NGC 147 and NGC 185. To a lesser extent, it is also the case for IC 10. This is interesting in light of its measured proper motion (Brunthaler et al. 2007). Thus, our model may be able to constrain $v_{f,M31}$. It prefers a value of 240.29 km/s, very close to the 240 km/s at which the prior distribution peaks (Table 2). We are unable to determine the precision with which our model constrains this parameter. We believe the suspiciously good agreement (within 0.03σ of the prior) indicates that our analysis is simply unable to obtain meaningful constraints on $v_{f,M31}$, such that its prior is the most important consideration.

Our analysis preferred a low value of $v_{c,\odot}$, so we focused on adjusting only this parameter to better constrain its optimal value. This did not alter our results. Our 3D analysis alone must prefer even lower values than the best fit, which also considers our prior of 240 ± 10 km/s. Given that analyses such as these typically constrain $v_{c,\odot}$ to within no better than ~ 15 km/s (e.g. Peñarrubia et al. 2014; Banik & Zhao 2016), it appears that there is some tension between the 223 km/s preferred by our analysis and the independent[1] estimate of 239 ± 5 km/s (McMillan 2011). Interestingly, a more recent estimate preferred a lower value (232.8 ± 3.0 km/s, McMillan 2016). However, the reduced uncertainty leads to the same conclusion.

Our model also contains some galaxies quite close to the MW, making it important to have an accurate force law within its virial radius. We may be failing to achieve this by assuming $v_{c,\odot} = v_f$, the speed at which the rotation curve of the MW flatlines. It is possible that the best-fitting LSR speed obtained by our algorithm has been dragged down because $v_f \ll v_{c,\odot}$. This is suggested by the work of Kafle et al. (2012). We hope to relax the assumption that $v_{c,\odot} = v_f$ in a future investigation.

Our axisymmetric analysis had almost no preference for a LSR speed different to the 239 km/s peak of its prior distribution (Table 2 of Banik & Zhao 2016). The lower value of $v_{c,\odot}$ preferred by our 3D analysis affects M, the inferred total mass of the MW and M31. This is because M31 is almost directly ahead of the Sun in its orbit around the MW. Thus, a lower LSR speed implies more of the observed blueshift of M31 must be due to it moving towards the MW, requiring a higher combined mass for these galaxies. This is also required to counteract the stronger effect of tides due to a higher inferred mass of Cen A, whose location very close to the MW-M31 line and relative proximity make it an important consideration. For these reasons, it is not too surprising that our 3D analysis prefers a higher M, even though this is counteracted slightly by the lower preferred distance to M31.

We conducted versions of our axisymmetric analysis without Cen A and with it included at a mass of $4 \times 10^{12} M_\odot$. The latter provided a much better fit to observations (Banik & Zhao 2016, Figure 14). Our 3D algorithm starts off with Cen A having $M_c = 1.06 \times 10^{13} M_\odot$ but the analysis prefers a value of just over half this (not problematic given the fairly broad mass priors − see Equation 18). This suggests the possibility of constraining the masses of galaxies just outside the LG based on their tidal effect within it. Such an analysis is likely to face degeneracies between masses of different galaxies along a similar line of sight, but it might still be worthwhile.

[1] not based on the timing argument

A comparison between our best-fitting 2D and 3D models is complicated somewhat by the latter having many more degrees of freedom. In particular, it is not required to match the observed distances of LG galaxies. This allows it to place a galaxy further away than observed, increasing its predicted GRV and better explaining a very high observed GRV. We handle this issue by applying a correction to model-predicted GRVs if they correspond to a simulated galaxy at a different distance than the real one it is supposed to represent. Thus, we set

$$GRV_{model} \rightarrow GRV_{model} + (d_{obs} - d_{model})\,\alpha H_0 \quad (23)$$

$$\alpha \equiv \frac{1}{H_0}\frac{dv_r}{dr} \quad (24)$$

We use $\alpha = 1.5$ because this seems to provide a reasonable estimate for how radial velocities v_r depend on distances within the LG (Figure 5). At long range, we would get $\alpha = 1$. Within the LG, gravity from the MW and M31 is important. Thus, an object further from them has been decelerated less by their gravity. This means that its radial velocity will be higher by a greater amount than in a homogeneously expanding Universe. Neglecting projection effects (which become small a few Mpc from the LG), we see that α should slightly exceed 1.

After obtaining corrected GRV predictions using Equation 23, we subtract them from observed GRVs (Equation 5) to obtain a list of ΔGRVs. We determine the root mean square (rms) of these ΔGRVs for a range of plausible assumptions regarding α. The precise value does not much affect our overall conclusions (Figure 7).

For comparison, we also show the result of the same calculation for our best-fitting 2D model using the same target galaxies. This model requires an extremely precise match between their simulated and observed distances, making the result independent of α. Instead, the main uncertainty concerns whether Cetus and DDO 216 are included in the analysis as they are very discrepant with this model. We suggest that they should not be included as they are quite close to M31 (Figure 1). If one also excludes them from the 3D analysis, then the rms value of ΔGRV for it is hardly affected (it rises $\sim$0.7 km/s), thus greatly exceeding the 2D result for the same sample. Even if these galaxies are included, any value of $\alpha > 1.1$ implies that the rms ΔGRV is larger in our 3D analysis.

Previously, we added an extra dispersion term to Equation 10 and marginalised over other variables to obtain a probability distribution for it (Banik & Zhao 2016). The most likely value we obtained (using the optimal LMC mass) was 40.43 km/s. Using the same target galaxies, the rms dispersion in ΔGRV with respect to the best-fitting 2D model is 40.65 km/s, almost exactly the same. This suggests that the two statistics are very similar, even though the former uses integration over model parameter space while the latter is based on just one model. Thus, the rms ΔGRV likely provides a very good guide to the results of a more thorough statistical analysis attempting to pin down how inaccurate our model is as a representation of the data.

Our previous work suggests that we can obtain error bars for Figure 7 using the usual rule for the uncertainty in the rms of N independent random variables. In this case, the fractional uncertainty when $N \gg 1$ is $\frac{1}{\sqrt{2N}}$, where the number of galaxies is $N = 34$. Thus, we expect an uncertainty

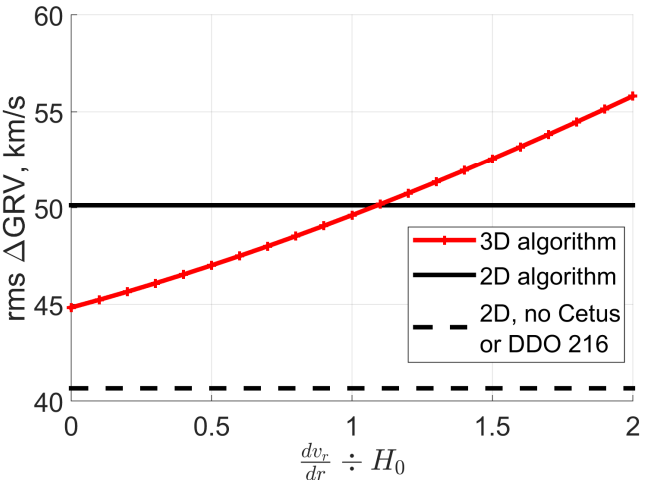

Figure 7. The root mean square value of ΔGRV is shown here for the best-fitting 2D (black) and 3D (red) models. α governs the way we adjust 3D model predictions to put them on an equal footing with our 2D model (Equation 23). This adjustment is unnecessary for the latter because it matches observed and simulated downrange distances of target galaxies to within 1 part in 10^5. This model is likely unreliable close to M31 as it lacks M33, making its predictions for Cetus and DDO 216 unreliable. Results including these galaxies (solid black) and without them (dashed black) are shown. In the 3D model, removing them increases the results by $\sim$0.7 km/s, leaving them almost unchanged.

of $\sim$6 km/s, making at least the 3D results inconsistent with the 30 km/s scatter about the Hubble flow found by Aragon-Calvo et al. (2011).

In order to estimate uncertainties more rigorously, we run another axisymmetric simulation with parameters chosen to match those in our best-fitting 3D model. This is only possible for some parameters (shown in Table 2) as several relate to particles unique to the 3D model and to motion in 3D.

Using this model, we obtain estimates of how much uncertainty there is on the predicted GRV of each target because of its uncertain position along the line of sight (Equation 8). To obtain the uncertainty on its ΔGRV, we also need to add in quadrature the uncertainty on its observed radial velocity σ_{v_h} (Equation 10).[1] We expect this to capture the major observational sources of error.

After determining ΔGRV and its uncertainty for each target with respect to our 3D model, we can readily see if any galaxies have an unusual redshift for their position. Neglecting a couple of galaxies with large distance uncertainties,[2] we show the 5 most extreme cases of anomalously high and low GRVs in Table 4. It is apparent that several galaxies have observed GRVs substantially different from that predicted by our best-fitting model.

Whatever specific scheme is used for softening the forces close to massive objects (e.g. Equation 14), there must be a transition to an inverse square law beyond a distance of

[1] The actual observational uncertainty is used, not 20 km/s.
[2] Leo P and NGC 404 have ΔGRVs of 72 ± 32 and 70 ± 38 km/s, respectively

Galaxy	ΔGRV (km/s)	Distance from LG barycentre (Mpc)
HIZSS 3	123.2 ± 10.6	1.76 ± 0.11
NGC 3109	110.7 ± 7.3	1.63 ± 0.05
Sextans A	95.1 ± 7.2	1.66 ± 0.02
Sextans B	75.4 ± 5.4	1.71 ± 0.05
Antlia	61.6 ± 8.3	1.68 ± 0.06
UGC 4879	-31.1 ± 5.5	1.32 ± 0.02
KKR 3	-33.6 ± 10.9	2.30 ± 0.12
GR 8	-40.0 ± 10.5	2.42 ± 0.12
NGC 55	-42.0 ± 10.4	2.08 ± 0.11
NGC 4163	-130.6 ± 7.7	2.96 ± 0.04

Table 4. ΔGRVs with respect to our 3D model for the LG galaxies most discrepant with it (excluding NGC 404 and Leo P due to large distance uncertainties, see text). Errors are estimated using Equation 10. The LG barycentre is put almost exactly at the MW-M31 mid-point (Table 2). Errors in the distance from there are obtained from those on heliocentric distances in the usual way.

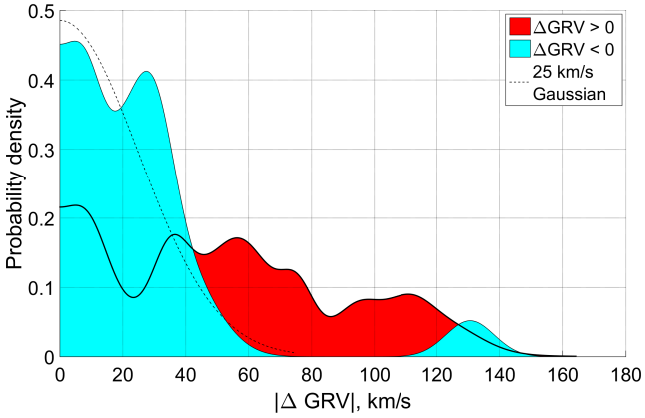

Figure 8. Histogram of ΔGRVs with respect to our 3D model, shown separately according to the sign of ΔGRV. The area of each square corresponds to 2 galaxies. A similar pattern emerges to Figure 3, with the blue bump near 130 km/s caused by NGC 4163. Otherwise, the galaxies with $\Delta GRV < 0$ (solid blue) are well described by a 25 km/s Gaussian (dashed line).

$r_S \sim \frac{GM}{v_f^2}$. This is only ~ 150 kpc for both the MW and M31. Thus, there can be little doubt about the force law further than ~ 1 Mpc from them, the region where the galaxies most discrepant with our model seem to lie (Table 4).

To gain a feel for the overall pattern of discrepancies between our model and observations, we construct a histogram of the ΔGRVs of our target galaxies using a similar procedure to that used for Figure 3. This is shown in Figure 8. Because there is some uncertainty in how to convert HRVs into GRVs due to imperfect knowledge of $v_{c,\odot}$, we add 5 km/s in quadrature to the other uncertainties. Although the 3D analysis uses a wider (10 km/s) prior on $v_{c,\odot}$, we choose to stick with the previous value to allow for easier comparison between the histograms.

We have treated NGC 3109 and Antlia as separate objects. However, they may be gravitationally bound (van den Bergh 1999). There are indications that they have recently interacted, based on observations of both NGC 3109 (Barnes & de Blok 2001) and Antlia (Penny et al. 2012). This is more likely if Antlia is a satellite of NGC 3109. The 41 ± 1 km/s difference in their GRVs and their 1.19° sky separation (corresponding to $\gtrsim 28$ kpc) are likely consistent with this scenario if their heliocentric distances are similar. The distance to Antlia was found to be 1.31 ± 0.03 Mpc by a study focusing exclusively on this galaxy (Pimbblet & Couch 2012), similar to the 1.286 ± 0.015 Mpc measured previously by Dalcanton et al. (2009). The range of published distances to NGC 3109 is wider than their formal uncertainties, but the most accurate one (based on Cepheid variables) is 1.300 ± 0.012 Mpc (Soszyński et al. 2006). Thus, these two galaxies are probably not much more than 40 kpc apart and may well be bound.

If it turns out that Antlia should not be treated as an independent object, then our overall conclusions should not be much affected because its ΔGRV is close to the typical ~ 50 km/s (Figure 7). As a result, the removal of Antlia[1] from our sample only reduces the rms value of ΔGRV by 0.30 km/s. In this case, the appearance of Table 4 would also remain similar, with Tucana taking the place of Antlia. Tucana has a ΔGRV of 60.3 ± 7.7 km/s and is located 1.07 ± 0.05 Mpc from the LG barycentre.

We did not put Leo P into Table 4 due to a 32 km/s uncertainty on its ΔGRV, almost entirely due to a rather uncertain distance of 1.72 ± 0.4 Mpc. This is derived from ground-based observations (McQuinn et al. 2013). However, a more accurate distance measurement has recently been made using the Hubble Space Telescope (1.62 ± 0.15 Mpc, McQuinn et al. 2015). Based on how GRV predictions in our axisymmetric model vary with the assumed distance to Leo P, we estimate that this increases its ΔGRV by ~ 9 km/s while reducing the error on it to only ~ 13 km/s.

Considering the large difference between simulated and observed distances to Leo P (ruled out at almost 4σ using the newer distance), we looked more closely into how much we should adjust its GRV prediction to make this correspond to its observed position. Normally, we use Equation 23 without worrying too much about the precise value of α as typical distance errors are small. This is not the case here. Assuming that our axisymmetric model (with the same parameters as our 3D model) provides a better guide to how GRV predictions are affected by line of sight distances, it appears that α is overestimated slightly for Leo P. A value of only 1.12 is more appropriate, implying that we reduced its GRV prediction too much to account for it being closer in reality than in the model. As a result, its ΔGRV is slightly smaller, with a best guess of 68 ± 13 km/s using the updated distance and method.

Our closer look into Leo P hardly changes our estimate of its ΔGRV from the 72 ± 32 km/s assumed in the rest of this work. However, the error budget is more than halved, making it as discrepant with our 3D model as Antlia and Tucana. Importantly, the small change to the result for Leo P and the almost negligible effect of removing Antlia from our sample both lend confidence that our results should not change too much with future improvements to the data and model. This is especially true when one considers that the data for Leo P is particularly inaccurate if using its old dis-

[1] almost 5 magnitudes fainter than NGC 3109 (McConnachie 2012, Table 3)

tance estimate (Figure 13). Almost all other galaxies have substantially smaller observational uncertainties.

5 DISCUSSION

Realising the difficulty faced by our axisymmetric model in explaining observations of the LG, we used a 3D model with many times more free parameters (Table 3). The model was also constrained using more observations, but a lot of these were given quite large uncertainties. For example, we gave all simulated galaxies a HRV error budget of 20 km/s and assumed a 10% distance uncertainty for the ones outside the LG (Equation 15). We also relaxed the requirement for galaxies to be following the Hubble flow at the start of our simulations (Equation 1). It is clear that our best-fitting 3D model has taken full advantage of this liberty (Figure 6).

As well as relaxing the constraints on our model in these ways, we used a higher value for the Hubble constant and treated the effect of cosmological acceleration differently (Equation 14). In our axisymmetric model, these changes generally increase the predicted GRVs of galaxies near the edge of the LG for fairly intuitive reasons, thus improving the fit to observations (Banik & Zhao 2016, Sections 4.1 and 4.2).

Despite altering our model and the constraints it faced in these ways, our best-fitting 3D model provides a similarly poor match to observations as our best-fitting axisymmetric model (Figure 7). Some dispersion amongst the ΔGRVs is expected due to observational and modelling uncertainties. Using a rigorous grid investigation of the model parameters, we showed previously that there is an unacceptably large typical mismatch between observations and predictions made by our axisymmetric model (Banik & Zhao 2016, Section 4). Similar conclusions would be obtained if focusing on the best-fitting model alone (Section 4). We assume that this is also true in our 3D model, justifying our focus on the best-fitting one.

Without a grid investigation of the parameters in our 3D model, one might be concerned whether a qualitatively different type of trajectory for some of the massive galaxies might alter the gravitational field in the LG so as to greatly improve the fit to observations. We consider this unlikely for a timing argument analysis such as ours. The reason is that any plausible solution has the MW and M31 turning around just once, while more distant objects outside the LG have not turned around. It is not feasible for the MW and M31 to have undergone a past close flyby in ΛCDM (or in our model) for any realistic total mass of these galaxies. Thus, the algorithm only needs to solve the continuous problems associated with determining when the turnaround occurred, what the present distance to M31 and its GRV are etc. It does not need to solve discrete problems like how many times the MW and M31 have turned around. This suggests that gradual adjustments to the model parameters should eventually converge on the best-fitting solution, as assumed in the rest of this work. However, it should be borne in mind that the solution presented here is preliminary and a better fit to the observations may eventually be obtained using our model.

Although our 2D and 3D models yield broadly similar conclusions, this is not always the case for individual galaxies. To compare the models in a more direct way, we ran our axisymmetric model using the same parameters as our best-fitting 3D model (Table 2), ignoring features unique to the latter. The GRV predictions of our 3D model were referred to the barycentre of the MW and LMC as the latter is absent from our 2D model and only included indirectly (Banik & Zhao 2016, Section 4.4).

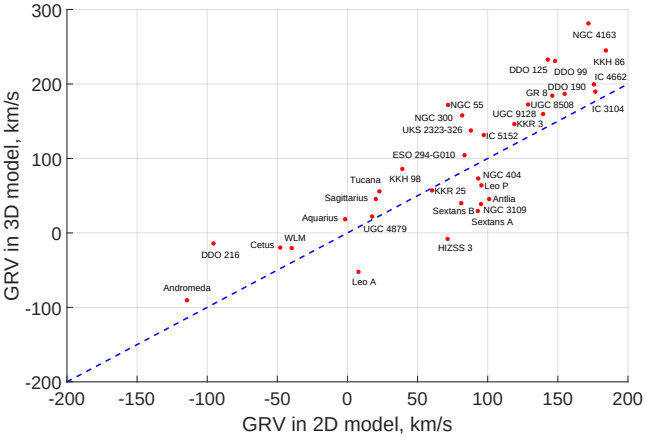

Figure 9. Comparison between model-predicted GRVs in our 2D and 3D models with the same model parameters (last column of Table 2). The line of equality is shown in blue.

Predictions from both models are compared in Figure 9 and a histogram of the differences between their GRV predictions is shown in Figure 10. The models broadly agree, with an average absolute difference of 44.6 km/s. Interestingly, the 3D results are biased higher by 20.4 km/s. Thus, the model with more free parameters will have more flexibility to increase predicted GRVs.

The main way in which this can be done is through adjusting the tides raised on the LG by objects outside it (Table 3). This leads to the Hubble diagram traced out by our 3D model showing slightly higher radial velocities towards the edge of the LG compared with our axisymmetric model (Figure 5). Of course, one also expects radial velocities to be reduced for objects in certain directions (Equation 25). We suppose our algorithm tries to ensure there are fewer target galaxies – especially those with a high ΔGRV – towards those directions.

As well as increased flexibility at long range, our 3D model should be more accurate close to the MW and M31 because it directly includes their most massive satellites. This is probably why it achieves a much better fit to the GRV of DDO 216, which is otherwise too high in our 2D model. In our 3D model, it has a close (73 kpc) encounter with M33 almost exactly 8 Gyr ago.

The overall distribution of ΔGRVs is shown in Figure 8 for our 3D model and in Figure 3 for our 2D model. Both models have a tendency for observed GRVs to exceed predicted ones. The pronounced bump near $\Delta GRV = 80$ km/s in the 2D model gives way to a much broader and shallower bump at a slightly lower ΔGRV with respect to our 3D model. Neglecting the bump near 160 km/s in the 2D results because it corresponds to DDO 216, the distribution of ΔGRVs extends to even higher values in the 3D model.

Some of the galaxies we identify as having high ΔGRV

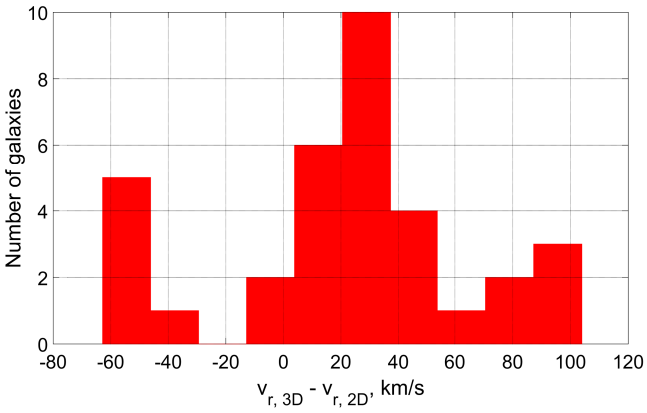

Figure 10. Histogram of the differences between GRV model predictions in the 2D and 3D models (former subtracted). The mean absolute difference is 44.6 km/s, with the 3D model predictions biased higher by 20.4 km/s on average.

have previously been identified as such. For example, Pawlowski & McGaugh (2014) identified NGC 3109, Antlia, Sextans A, Sextans B and Tucana as having anomalously high GRVs. With a slightly lower ΔGRV of 60.3 ± 7.7 km/s and a distance from the LG barycentre of 1.07 ± 0.05 Mpc, Tucana narrowly misses out on appearing in Table 3 but is significantly discrepant with our model.

These 5 objects have previously been identified as possible backsplash galaxies i.e. objects that have passed within the virial radius of the MW or M31 (Teyssier et al. 2012). There, they may have passed close to a massive satellite such as M33. Despite allowing for such trajectories, we are still unable to provide a good match to the observed GRVs of several LG dwarf galaxies. We also note that Peebles et al. (2011) found it very difficult to incorporate Sextans A and B into their dynamical model of the LG, suggesting that it could not easily explain their motions. Thus, the high velocity galaxy problem appears to persist even with a 3D model.

However, the most extreme outlier with respect to our model is actually a galaxy with negative ΔGRV. This is NGC 4163, a galaxy which appears unusual even in the almost model-independent analysis shown in Table 1. Here, it is apparent that two nearby galaxies have a much higher ΔGRV, suggesting that GRVs of galaxies near NGC 4163 are higher than its GRV. This is also apparent when considering the radial velocities of other galaxies at similar heliocentric distances in the Canes Venatici I cloud (Table 2 of Makarov et al. 2013). Thus, leaving aside any models, it appears that the HRV of NGC 4163 is ~ 100 km/s less than that of neighbouring galaxies.

One possible explanation is that NGC 4163 was flung towards the LG as a result of a gravitational slingshot interaction in a nearby galaxy group. It is also possible that NGC 4163 had a more recent interaction with a galaxy close to it, as perhaps suggested by its recent starburst (McQuinn et al. 2009). In fact, our 3D model has DDO 99 passing within 50 kpc of it, although this happened in ancient times (when $a = 0.32$). Nonetheless, it is possible that our model has got the timing of this encounter wrong, especially as it does not simulate the effects of any such encounter because both galaxies are treated as test particles. Certainly such a close encounter is rare in our models. If it did happen, then the fact that NGC 4163 is almost a magnitude fainter (McConnachie 2012) suggests that its dynamics would be affected to a greater extent. Thus, several explanations are possible for its anomalously low GRV.

Interactions amongst galaxies in a neighbouring group can fling a galaxy towards the LG, leading to a galaxy with anomalously low GRV. However, it is very difficult to explain a galaxy with anomalously high GRV in this way. This is possible only if the galaxy has crossed the LG and is now heading away from it again. It is not feasible for a galaxy like NGC 3109 to cover such a large distance in the time since the Big Bang. To see why, consider that it is 1.6 Mpc from the LG, such that the Hubble velocity is ~ 110 km/s. Given an extra radial velocity of 120 km/s, we see that the galaxy can have covered perhaps twice as much distance as a typical galaxy on the Hubble flow. This means that the anomalous motion of NGC 3109 could not have originated much further from the LG than its present distance, albeit on the opposite side (Equation 37).

Furthermore, even if this scenario was plausible, it is clear that it would be rarer than a situation where a galaxy is flung towards the LG and we observe it on the way in. Thus, we might see several galaxies with anomalously high GRV, but we would expect to see even more with anomalously low GRV. The opposite seems to be the case (Figure 8).

Using a 3D model, we can quantify how fast target galaxies move out of the plane they define with the MW and M31. Referring velocities to the barycentre of the MW and LMC, we obtain the results shown in Figure 11. Part of the reason for such non-axisymmetric motion is that the MW and M31 are not on a purely radial orbit. However, this is only a ~ 30 km/s effect (van der Marel et al. 2012b). Thus, the explanation must lie mostly with the non-axisymmetric gravitational field caused by massive objects far from the MW−M31 line. Massive satellite galaxies such as the LMC and M33 must also play a role.

The substantial non-axisymmetric motions suggested by our analysis are probably required in order to boost the centrifugal force, helping explain the high GRVs of several LG galaxies. Some of this tangential motion may be a relic of peculiar velocities at the start of our simulation (Figure 6), especially when considering that Hubble drag does not dissipate specific angular momentum (Equation 10 of Banik & Zhao 2016). Although the expansion of the Universe naturally reduces tangential speeds, this is not as important an effect as one might think. For example, our best-fitting 3D model has NGC 3109 starting off 593 kpc from the MW and being 1.37 Mpc away currently. Its distance has increased $< 2.5\times$ despite the Universe overall having expanded by a factor of 10.

In future, such non-axisymmetric motions should become detectable based on proper motion measurements. A good target for this may be DDO 216 due to its relative proximity. Our model implies it had a past close encounter with M33, constraining the possible trajectories of these two galaxies and also indirectly forcing some limits on the past position of M31.

The larger expected out-of-plane velocities of Cetus and Tucana should make their proper motions similar in magnitude to that of DDO 216, despite a greater distance. Tu-

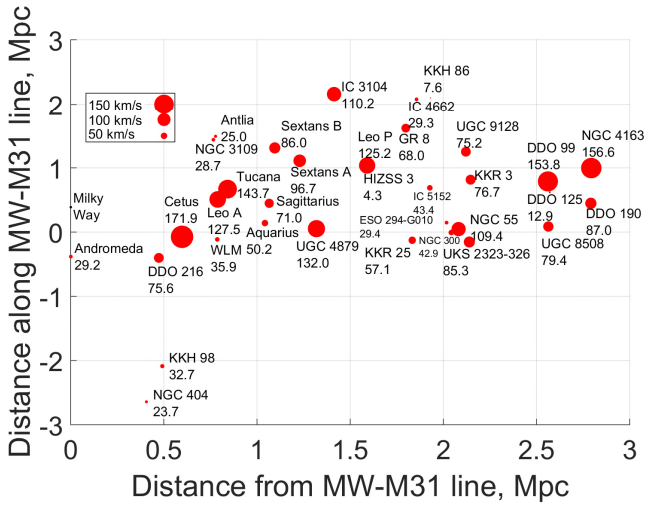

Figure 11. Velocities of our target galaxies out of the plane they define with the MW and M31 are shown here using marker sizes. This information is also given as a number (km/s) below the corresponding galaxy name. Galaxy positions are shown relative to the MW−M31 line.

cana is one of the nearest galaxies with an unusual GRV in our analysis. But several galaxies with much larger ΔGRV lie just a little further away, in the vicinity of NGC 3109 (Figure 13). Its proper motion promises to be an extremely interesting constraint on any models of the LG (Pawlowski & McGaugh 2014).

5.1 Effect of the Great Attractor

A 3D model including several objects beyond the LG allows for a much more rigorous handling of the tides they raise within it. Such effects tend to be larger at greater distances. Thus, it is interesting that the most discrepant objects found by our previous axisymmetric analysis tend to lie towards the edge of the LG (Banik & Zhao 2016, Figure 10). A similar trend is apparent when the LMC is included indirectly (Figure 2), bearing in mind that a high GRV generally implies a greater distance and that the absence of M33 from the model makes it less reliable for galaxies such as Cetus and DDO 216 which are close to M31.

In our 3D model, despite handling tides more rigorously, we found a similarly poor match between observed and model-predicted GRVs (Figure 7). However, the model does not include all the mass concentrations outside the LG which may be relevant to our analysis. An important example is the Great Attractor (GA, Mieske et al. 2005). This is thought to be primarily responsible for the $\sim$630 km/s magnitude of $\boldsymbol{v}_{pec,LG}$, the velocity of the LG as a whole with respect to the surface of last scattering (Kogut et al. 1993).

To estimate the effect of the GA on GRVs of objects within the LG, we use the distant tide approximation. Treating LG galaxies as freely falling in the gravitational field of a distant point mass, the change in the GRV of a target galaxy due to the GA is given by

$$\Delta GRV_{GA} = \left(3\cos^2\theta - 1\right)\beta_{IC}\frac{v_{pec,LG}\,d}{d_{GA}} \quad \text{for } d \ll d_{GA} \quad (25)$$

d_{GA} is the distance to the GA while θ is the angle on our sky between it and the target galaxy, which is at a heliocentric distance d. The parameter $\beta_{IC} \approx 0.76$ accounts for an effect similar to Hubble drag.

We assume the GA caused the LG to gain a peculiar velocity of $v_{pec,LG} = 630$ km/s. The direction towards the GA is taken to be $l = 325°$, $b = -7°$ in Galactic co-ordinates (Kraan-Korteweg 2000). This is similar to the direction of $\boldsymbol{v}_{pec,LG}$. The discrepancy is likely caused by less massive objects closer to the LG. For example, Centaurus A, M81 and IC 342 are all in the northern Galactic hemisphere, partly explaining why $\boldsymbol{v}_{pec,LG}$ points further north than the direction towards the GA.

Tides raised by the GA on the LG cause two objects in it to end up with a different present relative position than if the GA did not exist. Thus, if we know the present position of e.g. IC 3104, then its initial position must be different depending on whether the GA is included in our model. Assuming IC 3104 is located directly towards the GA, it needs to start closer to the MW if the GA is included, partly cancelling the GRV-raising effect of the GA. This 'initial condition drag' leads to an extra factor of $\beta_{IC} < 1$ in Equation 25.

To estimate β_{IC}, we construct a basic simulation involving a particle of mass M in an otherwise homogeneous Universe. A test particle a distance r away is required to satisfy $r = d$ with a peculiar velocity close to 630 km/s at the present time. This is achieved by varying its position when the cosmic scale-factor $a = 0.1$, at which time the particle satisfied Equation 1. In Section 2.1 of Banik & Zhao (2016), we used General Relativity to show that the test particle satisfies

$$\ddot{r} = \frac{\ddot{a}}{a}r - \frac{GM}{r^2} \quad (26)$$

We solve this problem using a Newton-Raphson procedure targeting a present distance of $d = 84$ Mpc. We then repeat the calculation with a slightly different d. Without the GA, the relative radial velocity of the particles would be $H_0 r$. Thus, we determine the effect of the GA using

$$\Delta GRV_{GA} = \Delta v_{pec} \quad \text{where} \quad (27)$$

$$v_{pec} \equiv \dot{r} - H_0 r \quad (28)$$

In this way, we find that $\beta_{IC} \approx 0.76$ for both the cosmological models given in Table 2. Assuming ΔGRV_{GA} has the same angular dependence as the tidal field that causes it, we suppose that this calculation is sufficient to determine the result for all angles θ. This should be valid as long as the tides raised by the GA can be approximated as linear in position, which is reasonable within the LG.

For θ close to 0 or 180°, the GA tends to increase GRVs. However, for θ close to 90°, the GA reduces GRVs. This is because both the MW and the target galaxy accelerate towards the perturber at similar rates. As their co-moving distance from the GA decreases, so also does their co-moving distance from each other. Thus, the GA can only increase GRVs along one direction. It must reduce them along the other two, albeit by half as much. This is due to the divergence-free nature of the gravitational field far from its source. As a result, an external tidal field on the LG does not readily resolve the high velocity galaxy problem within it as these galaxies lie in several quite different sky directions (Table 4).

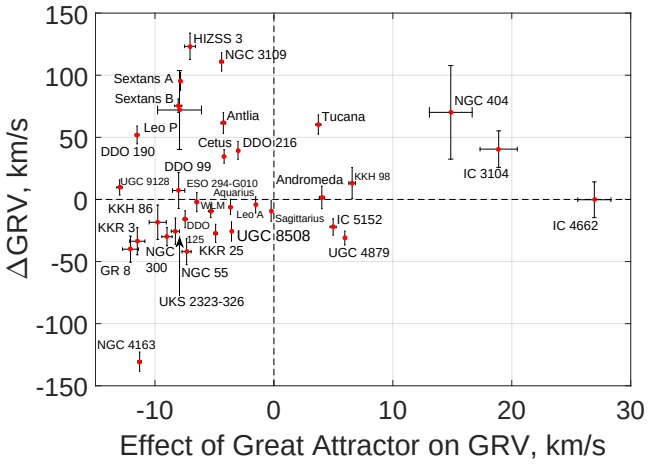

Figure 12. ΔGRVs are shown against our estimate for how much the Great Attractor might have increased the GRV of each galaxy (Equation 25). Errors are correlated because a larger distance increases the effect of the GA while reducing ΔGRV.

Nonetheless, one can hope that the GA helps with some of the most problematic targets. To see if this is the case, we compare the effect of the GA predicted by Equation 25 and the ΔGRV of each galaxy. This is shown in Figure 12. Here, we have propagated distance uncertainties in the usual way. The error budget on each ΔGRV accounts for uncertainties in the corresponding HRV and distance measurements (Equation 10). A different GA distance to the assumed 84 Mpc causes a rescaling of its effects.

Equation 25 suggests that the GA should actually have *reduced* the GRV of most or all of the galaxies with the highest ΔGRV (listed in Table 4). This remains the case if Antlia is treated as a low mass satellite of NGC 3109 and excluded from our sample (van den Bergh 1999). Thus, far from helping to solve the high velocity galaxy problem, the GA appears to make it worse.

As for galaxies with $\Delta GRV < 0$, only one galaxy has a GRV so low as to be problematic given the expected ∼25 km/s accuracy of our model. This is NGC 4163, which we have discussed previously. Our results suggest that its GRV would be reduced by the GA, thus helping to explain its low observed GRV. However, the effect is almost an order of magnitude too small.

It is straightforward to consider all the LG target galaxies in our sample, not just those substantially discrepant with our best-fitting model. After adjusting GRV predictions for the GA using Equation 25 with different assumptions regarding the parameter α (Equation 23), we found that the rms ΔGRV increased very slightly.

$$\text{Increase in rms } \Delta GRV \;\approx\; (0.84 - 0.36\alpha)\ \text{km/s} \qquad (29)$$

The very small effect of the GA on the rms ΔGRV could well be a sign that our algorithm has utilised its many degrees of freedom to adjust the tidal field acting on the LG so as to best match observations.

Taken at face value, our analysis suggests that even galaxies at the edge of the LG ∼3 Mpc away would only have $\Delta GRV_{GA} \sim 35$ km/s at most. Typical effects would be $\sim \frac{1}{4}$ as much due to smaller distances and projection effects. Considering that several galaxies have a much larger ΔGRV such that even its rms value exceeds 40 km/s, the effect of the GA is too little to substantially alter our conclusions.

However, cosmological simulations based on ΛCDM suggest that structure tends to form along filaments (e.g. Springel et al. 2005, Figure 1). Thus, there may well be additional structures along the line of sight towards the GA (or on the opposite side) at smaller distances. The effect of these structures on the LG would be similar to that of the GA, but with an increased magnitude due to the smaller distance. This suggests that we may have underestimated the effects shown in Figure 12.

So far, we assumed that the GA has always been in the same direction. Due to its large distance, it is almost certainly very close to the Hubble flow today. This was likely the case over the vast majority of the age of the Universe. It may not have been so at early times. However, because of Hubble drag, gravitational forces then have only a very small effect on present peculiar velocities (e.g. Banik & Zhao 2016, Figure 4). Thus, the crucial ingredient in predicting how the LG should be affected by the GA is its present position.

5.2 Modified Gravity

The high GRVs of some LG galaxies must have been caused by forces acting on them which our model does not account for. The nature of these forces might be better understood if we had an idea of the spacetime location where they acted. Thus, it is necessary to estimate where some of these galaxies may have been. For the sake of clarity, we will focus on NGC 3109 because it has a high ΔGRV in our model (Table 4) and was also identified as having a rather high GRV in previous works (Pawlowski & McGaugh 2014; Teyssier et al. 2012).

In this regard, it is helpful to define co-moving positions $\boldsymbol{x}$ which do not change for particles in a homogeneous Universe. Thus, they are related to physical positions $\boldsymbol{r}$ by

$$\boldsymbol{x} \;\equiv\; \frac{\boldsymbol{r}}{a} \qquad (30)$$

As we are dealing with unknown forces, we only seek a rough estimate of the co-moving displacement d of NGC 3109. We assume it is so distant as to be following the Hubble flow in our model, such that $d \approx 0$ in it. The actual value of d is estimated based on integrating the trajectory of NGC 3109 backwards in time, with the effect of gravity crudely included by using its ΔGRV instead of its actual peculiar velocity as a present boundary condition. For simplicity, we only consider motion along the line between the LG barycentre and the present position of NGC 3109. Thus, its present peculiar velocity (Equation 28) for the purposes of this section is estimated as

$$v_{pec,0} \;\approx\; \Delta GRV \qquad (31)$$

Due to the effect of Hubble drag (e.g. Banik & Zhao 2016, Equation 24), the peculiar velocity of a free particle changes with time according to $v_{pec} \propto a^{-1}$. Furthermore, even the same peculiar velocity corresponds to a more rapidly changing co-moving position in the past (Equation 30). Thus, integrating between some past time t_i and the

present time t_0, we estimate that

$$d = \int_{t_i}^{t_0} \frac{v_{pec}}{a}\, dt \quad (32)$$

$$= \int_{t_i}^{t_0} \frac{v_{pec,0}}{a^2}\, dt \quad (33)$$

$$= \int_{a_i}^{1} \frac{v_{pec,0}}{a^2 \dot{a}}\, da \quad (34)$$

$$(35)$$

For a rough estimate, it is acceptable to approximate the expansion history of the Universe (Equation 3) using

$$a \approx H_0 t \quad (36)$$

During the time period of interest ($a \gtrsim 0.2$), the results obtained in this way for $\int_{t_i}^{t_0} a^{-2}\, dt$ are accurate to within $\sim 10\%$.[1] This allows us to solve Equation 35.

$$d = \frac{v_{pec,0}}{H_0}\left({a_i}^{-1} - 1\right) \quad (37)$$

$$= \frac{v_{pec,0} z}{H_0} \quad \text{where} \quad (38)$$

$$z \equiv \left({a_i}^{-1} - 1\right) \quad (39)$$

To simplify our discussion, we assume that the high ΔGRV of NGC 3109 was caused by forces acting over a small fraction of the Hubble time, e.g. due to an encounter with a massive object. There is a trade-off between how long ago these forces acted and their total impulse. M31 is the fastest rotating LG galaxy, with a circular velocity of ~ 225 km/s (Carignan et al. 2006). An impulse of twice this is only possible for an object not eventually accreted if it is on a circular orbit. Thus, we suppose that the impulse could not feasibly have exceeded triple the ~ 110 km/s ΔGRV of NGC 3109, implying $a_i > \frac{1}{3}$. In the limiting case, an unexplained impulse of ~ 330 km/s would have to be acquired when the redshift $z = 2$, presumably in a gravitational interaction.

Given that 110 km/s is very close to the Hubble flow rate at the distance of NGC 3109, we can set $v_{pec,0} \approx H_0 d_0$, where the present co-moving/physical distance from the LG barycentre to NGC 3109 is d_0. Thus, its co-moving displacement d could not have much exceeded twice this, in which case the unexplained impulse occurred $\lesssim 1.7$ co-moving Mpc from the LG on the opposite side to where NGC 3109 currently lies. This makes it very difficult to understand how the present motion of NGC 3109 came about if one looks for an explanation outside the LG. Furthermore, the effect of gravity implies that galaxy groups outside it must have started at a slightly larger co-moving separation with it than they presently have. For example, our model indicates that the co-moving distance between the MW-M31 mid-point and Cen A has decreased from 4.98 Mpc to 4.04 Mpc since redshift 9.

A more plausible scenario might be that the MW and/or M31 are the massive object(s) responsible for the anomalous kinematics of NGC 3109. In this case, the missing ingredient is an impulse close to the LG barycentre, since which time the co-moving displacement $d \approx d_0$. For this to occur, we need to set $a_i = \frac{1}{2}$ in Equation 37, corresponding to ~ 8 Gyr ago. The conclusion that NGC 3109 was likely close to the LG barycentre at this time has previously been reached using simpler methods (Pawlowski & McGaugh 2014).

However, it would be very unusual if the major LG galaxies were responsible for the high ΔGRV of NGC 3109. After all, our model directly includes the MW and M31 as well as their most massive satellites (Table 3). Nonetheless, gravitational slingshot interactions with these objects could well lead to high GRVs, as occurs close to the LG barycentre (bottom panel of Figure 1). Thus, increasing the efficiency of this process might help to explain the observations. The energy gained in such interactions is reliant on the gravitational potential of the massive body being time-dependent due to its motion. This suggests that the relative motion of the MW and M31 might have been much faster in the past than implied by our model. Given their known relative velocity at present, this implies a rather high mutual acceleration. Therefore, we need to consider whether we have correctly understood the gravitational effect of the MW and M31 on each other.

So far, our discussion has been restricted to models based on ΛCDM. We have seen that it faces difficulties in explaining the dynamics of LG galaxies, both using a 3D model and a thorough grid investigation of the parameters in an axisymmetric model (Banik & Zhao 2016).

Beyond the LG, some remarkably tight correlations exist between the dynamics of galaxies and the distribution of their luminous matter (e.g. Famaey & McGaugh 2012, and references therein). These were unexpected in the context of ΛCDM. However, many of the trends were predicted a priori using Modified Newtonian Dynamics (MOND, Milgrom 1983). Thus, we consider whether this theory may shed light on the high velocity galaxy problem. Our reasoning will be similar to that in Section 4.6 of Banik & Zhao (2016).

MOND imposes an acceleration-dependent modification to the usual Poisson Equation of Newtonian gravity (Bekenstein & Milgrom 1984). In spherical symmetry, the result is that the gravitational field g at distance r from an isolated point mass M transitions from the usual inverse square law at short range to

$$g = \frac{\sqrt{GMa_0}}{r} \quad \text{for} \quad r \gg \frac{\sqrt{GM}}{a_0} \quad (40)$$

Here, a_0 is a fundamental acceleration scale of nature. Empirically, its value must be close to 1.2×10^{-10} m/s^2 to match galaxy rotation curves (McGaugh 2011). At this value, there is a remarkable coincidence with the acceleration at which the energy density in a classical gravitational field becomes comparable to the dark energy density u_Λ.[2] Thus,

$$\frac{g^2}{8\pi \mathrm{G}} < u_\Lambda c^2 \Leftrightarrow g \lesssim 2\pi \mathrm{a_0} \quad (41)$$

This suggests that MOND may be caused by quantum gravity effects (e.g. Milgrom 1999; Pazy 2013). Regardless of the underlying microphysical explanation, at sufficiently low acceleration, MOND gravity from a point mass follows Equation 40 as long as gravity from other objects is negligible.

[1] A much smaller error is achieved if a_i is close to 0.2 or 1.

[2] Dark energy is required to explain why $\ddot{a} > 0$ despite the attractive effect of gravity (Riess et al. 1998).

The external gravitational field on the LG can be estimated based on its peculiar velocity of ~ 630 km/s relative to the surface of last scattering (Planck Collaboration 2014). As might be expected, this shows the LG to be fairly isolated (Famaey et al. 2007). Thus, the force between the MW and M31 declines much slower with their separation than in ΛCDM, especially in the range between their virial radii (~ 150 kpc in our models) and their actual separation (783 ± 25 kpc, McConnachie 2012).[1]

If correct, the much stronger force between these galaxies has dramatic consequences, not just for their evolution but also for the rest of the LG. This is because the MW−M31 orbit is almost radial (van der Marel et al. 2012b). As a result, MOND implies a past close flyby encounter between them 9 ± 2 Gyr ago (Zhao et al. 2013). The tidal tails expelled from the disks of these galaxies during their interaction may be responsible for the thin co-rotating system of satellites around the MW (e.g. Pawlowski & Kroupa 2013) and the similar system around M31 (Ibata et al. 2013). This interaction may also have formed the thick disk of the MW (Gilmore & Reid 1983), a structure which seems to have formed fairly rapidly from the thin disk 9 ± 1 Gyr ago (Quillen & Garnett 2001). More recent investigations also suggest a fairly rapid formation timescale (Hayden et al. 2015). The disk heating which likely formed the thick disk appears to have been stronger in the outer parts of the MW, characteristic of a tidal effect (Banik 2014).

At the point of closest approach, the relative velocity of the MW and M31 would have been ~ 600 km/s (Zhao et al. 2013). Such fast motions could lead to very powerful gravitational slingshot encounters. The limiting factor might even have been their circular rotation velocities rather than the motions of their centres of mass. If we assume a maximum impulse of $\sim v_{f,M31}$ and an encounter when $a_i = \frac{1}{2}$, then it is easy to see why there are no galaxies with $\Delta GRV \gtrsim 120$ km/s.

For this explanation to work, the galaxies with a high GRV in our ΛCDM-based model need to have been flung out from close to the LG barycentre at around the time the MW and M31 had their interaction. This implies that galaxies with a higher ΔGRV should generally lie further away from the LG. Thus, it is interesting that the conclusions we reached above using NGC 3109 also hold with Tucana because its lower ΔGRV is compensated by a smaller distance from the LG. This can be seen visually if one draws a line through these galaxies on Figure 13 and realises that it passes close to the origin. The $\Delta GRV \lesssim d$ relation between velocities and distances d from the LG barycentre also seems to apply to HIZSS 3, Sextans A and Sextans B. In theory, it applies to Cetus and DDO 216, though their low values of ΔGRV meay mean that this is just a coincidence. Antlia falls slightly below this relation, but its GRV may have been reduced due to the effects of NGC 3109. Tidal features in it suggest that the two may have already undergone a pericentre (Barnes & de Blok 2001). The distance to Leo P is still sufficiently uncertain that it is consistent with the $\Delta GRV \lesssim d$ relation.

[1] At still greater distances, the force would transition to the usual inverse square law, but with a much higher normalisation (Milgrom 1986).

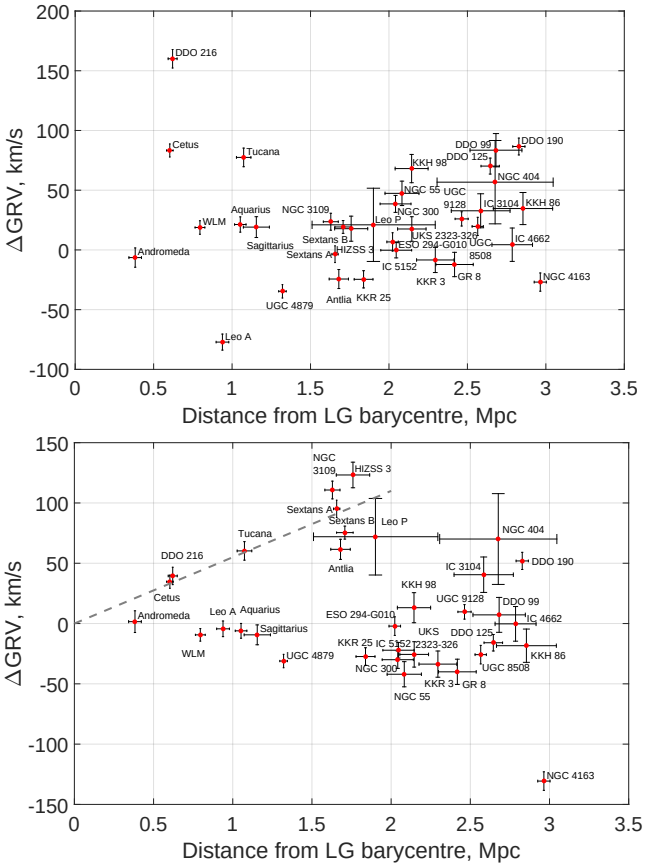

Figure 13. ΔGRV is shown for our target galaxies against their distance from the LG barycentre. Parameters of the models used are given in Table 2, with the best-fitting ones used for the relevant number of dimensions in the model. Errors shown tend to be anti-correlated because a larger distance to a target increases its predicted GRV, reducing its ΔGRV. *Top:* 2D model. *Bottom:* 3D model.

NGC 404 appears to have just as large a ΔGRV as some of the galaxies just considered, despite being further from the LG. However, we showed in Section 5.1 that its GRV has likely been increased by ~ 20 km/s due to the GA. Thus, although the nominal 3.06 Mpc distance we used seems to be correct (Dalcanton et al. 2009), its GRV is not that unusual in a ΛCDM context.

It is interesting that out of the 18 targets we have at distances of 2−3 Mpc from the LG barycentre, all of them are broadly consistent with expectations based on ΛCDM because none of them have a 1σ lower bound on their ΔGRV exceeding 60 km/s. However, at least 4 galaxies like this exist at distances of 1−2 Mpc, despite only having 11 targets in this range. The hypothesis that such high velocity galaxies are equally likely to exist in both distance bins can be ruled out at the 3σ confidence level. This suggests that the mechanism missing from our models can only cause high ΔGRVs out to ~ 2 Mpc, quite unlike the effect of tides (which should be even stronger at greater distances). Consequently, we favour an explanation inside the LG and suggest that the crucial ingredient missing from our models is a past MW-M31 flyby.

6 CONCLUSIONS

We construct axisymmetric and three-dimensional dynamical models of the Local Group (LG) in the ΛCDM standard cosmological model. Neither is able to provide a good match to the observed positions and velocities of galaxies within $\sim$1−3 Mpc of the LG barycentre (Figure 7). This is despite our 3D model accounting for quite a large number of massive objects both within and outside the LG (Table 3) with fairly weak prior constraints on their masses (Equation 18).

Both analyses reveal several galaxies with radial velocities (RVs) much higher than model predictions. However, galaxies with anomalously low RVs are rare (Figures 3 and 8). Thus, the high velocity galaxy problem within the LG persists when using a 3D model for it.

In the framework of ΛCDM, our axisymmetric and 3D results suggest that the past motions of the MW and M31 are too slow to explain the observed kinematics of LG galaxies. A similar challenge with high velocity objects also exists in some systems far outside the LG. For example, the high relative velocity of the components of the Bullet Cluster (Tucker et al. 1995) is difficult to reconcile with the gravity of their dark matter halos acting over the age of the Universe (e.g. Thompson & Nagamine 2012; Kraljic & Sarkar 2015). The latter analysis made careful use of extreme value statistics to handle the non-Gaussian nature of the tails of the probability distribution, perhaps explaining why it obtained different conclusions to the earlier work of Lage & Farrar (2015).

An explanation for the Bullet Cluster and other similar objects like El Gordo (Molnar & Broadhurst 2015; Ng et al. 2015) might well require a modification to our understanding of gravity on large scales. Indeed, cosmological N-body simulations in Modified Newtonian Dynamics (MOND, Milgrom 1983) could give rise to much higher pair-wise velocities (Llinares et al. 2009; Angus & Diaferio 2011).

Closer to home, MOND requires that the MW and M31 have undergone a past close flyby (Zhao et al. 2013). This is a consequence of their much stronger mutual gravitational attraction and the almost radial nature of their orbit (van der Marel et al. 2012b). Their higher relative velocity would likely help to explain observations of other LG galaxies.

Another interesting idea is that of dark matter as a superfluid (Berezhiani & Khoury 2016; Khoury 2016). In this model, phonons in this superfluid mediate forces between the baryons in a galaxy. This leads to MOND-like behaviour, helping to explain the observed tight correlation between the distribution of baryons in galaxies and their rotation curves (e.g. Famaey & McGaugh 2012, and references therein).

However, galaxies still need to be surrounded by large ($\sim$200 kpc) halos of dark matter in the normal phase to account for weak lensing because the phonon-mediated force does not affect photon trajectories. Thus, the strong galaxy-galaxy weak lensing signal (e.g. Brimioulle et al. 2013; Milgrom 2013) needs to be explained in much the same way as in ΛCDM. This means that interacting galaxies must experience strong dynamical friction between their dark matter halos. As a result, the MW and M31 could never have approached closely in the context of this model because they would subsequently merge.

We suggest that such an interaction nonetheless occurred and would help to resolve the high velocity galaxy problem in the LG. More work will be required to test this scenario.

The authors wish to thank P.J.E. Peebles for providing the algorithm used in this contribution. IB is supported by the Science and Technology Facilities Council.

REFERENCES

Alcock C., et al., 2000, ApJ, 542, 281
Angus G. W., Diaferio A., 2011, MNRAS, 417, 941
Aragon-Calvo M. A., Silk J., Szalay A. S., 2011, MNRAS, 415, L16
Banik I., 2014, preprint, Arxiv (arXiv:1406.4538v2)
Banik I., Zhao H., 2016, MNRAS, 459, 2237
Barnes D. G., de Blok W. J. G., 2001, AJ, 122, 825
Begum A., Chengalur J. N., Karachentsev I. D., Sharina M. E., 2005, MNRAS, 359, L53
Bekenstein J., Milgrom M., 1984, ApJ, 286, 7
Berezhiani L., Khoury J., 2016, Physics Letters B, 753, 639
Brimioulle F., Seitz S., Lerchster M., Bender R., Snigula J., 2013, MNRAS, 432, 1046
Brunthaler A., Reid M. J., Falcke H., Henkel C., Menten K. M., 2007, A & A, 462, 101
Carignan C., Chemin L., Huchtmeier W. K., Lockman F. J., 2006, ApJL, 641, L109
Carr B., 1994, ARA&A, 32, 531
Dalcanton J. J., et al., 2009, ApJS, 183, 67
Famaey B., McGaugh S. S., 2012, Living Reviews in Relativity, 15, 10
Famaey B., Bruneton J.-P., Zhao H., 2007, MNRAS, 377, L79
Fermi-LAT Collaboration 2015, Physical Review Letters, 115, 231301
Francis C., Anderson E., 2014, Celestial Mechanics and Dynamical Astronomy, 118, 399
Gilmore G., Reid N., 1983, MNRAS, 202, 1025
Harris G. L. H., Rejkuba M., Harris W. E., 2010, PASA, 27, 457
Hayden M. R., et al., 2015, ApJ, 808, 132
Ibata R. A., et al., 2013, Nature, 493, 62
Kafle P. R., Sharma S., Lewis G. F., Bland-Hawthorn J., 2012, ApJ, 761, 98
Kallivayalil N., van der Marel R. P., Besla G., Anderson J., Alcock C., 2013, ApJ, 764, 161
Khoury J., 2016, Physical Review D, 93, 103533
Kogut A., et al., 1993, ApJ, 419, 1
Kraan-Korteweg R. C., 2000, in Page D., Hirsch J. G., eds, Lecture Notes in Physics, Berlin Springer Verlag Vol. 556, From the Sun to the Great Attractor. p. 301 (arXiv:astro-ph/0006199)
Kraljic D., Sarkar S., 2015, JCAP, 4, 050
LUX Collaboration 2016, preprint, Arxiv (arXiv:1608.07648)
Lage C., Farrar G. R., 2015, JCAP, 2, 038
Llinares C., Zhao H. S., Knebe A., 2009, ApJL, 695, L145
Ma J., Wu Z., Wang S., Fan Z., Zhou X., Wu J., Jiang Z., Chen J., 2010, PASP, 122, 1164
Makarov D. I., Makarova L. N., Uklein R. I., 2013, Astrophysical Bulletin, 68, 125
McConnachie A. W., 2012, AJ, 144, 4
McGaugh S. S., 2011, Physical Review Letters, 106, 121303
McMillan P. J., 2011, MNRAS, 414, 2446
McMillan P. J., 2016, preprint, Arxiv (arXiv:1608.00971)
McQuinn K. B. W., Skillman E. D., Cannon J. M., Dalcanton J. J., Dolphin A., Stark D., Weisz D., 2009, ApJ, 695, 561
McQuinn K. B. W., et al., 2013, AJ, 146, 145
McQuinn K. B. W., et al., 2015, ApJ, 812, 158
Mieske S., Hilker M., Infante L., 2005, A&A, 438, 103
Milgrom M., 1983, ApJ, 270, 365

Milgrom M., 1986, ApJ, 302, 617
Milgrom M., 1999, Phys. Lett. A, 253, 273
Milgrom M., 2013, Physical Review Letters, 111, 041105
Molnar S. M., Broadhurst T., 2015, ApJ, 800, 37
Ng K. Y., Dawson W. A., Wittman D., Jee M. J., Hughes J. P., Menanteau F., Sifón C., 2015, MNRAS, 453, 1531
Ostriker J. P., Peebles P. J. E., 1973, ApJ, 186, 467
Pawlowski M. S., Kroupa P., 2013, MNRAS, 435, 2116
Pawlowski M. S., McGaugh S. S., 2014, MNRAS, 440, 908
Pazy E., 2013, Phys. Rev. D, 87, 084063
Peñarrubia J., Ma Y.-Z., Walker M. G., McConnachie A., 2014, MNRAS, 443, 2204
Peñarrubia J., Gómez F. A., Besla G., Erkal D., Ma Y.-Z., 2016, MNRAS, 456, L54
Peebles P. J. E., Tully R. B., 2013, preprint, Arxiv (arXiv:1302.6982)
Peebles P. J. E., Tully R. B., Shaya E. J., 2011, preprint, Arxiv (arXiv:1105.5596)
Penny S. J., Pimbblet K. A., Conselice C. J., Brown M. J. I., Grützbauch R., Floyd D. J. E., 2012, ApJL, 758, L32
Pietrzyński G., et al., 2013, Nature, 495, 76
Pimbblet K. A., Couch W. J., 2012, MNRAS, 419, 1153
Planck Collaboration 2014, A & A, 571, A27
Planck Collaboration 2015, preprint, Arxiv (arXiv:1502.01589)
Quillen A. C., Garnett D. R., 2001, in Funes J. G., Corsini E. M., eds, Astronomical Society of the Pacific Conference Series Vol. 230, Galaxy Disks and Disk Galaxies. pp 87–88
Riess A. G., et al., 1998, AJ, 116, 1009
Sandage A., 1986, ApJ, 307, 1
Schmidt K. H., 1958, Astronomische Nachrichten, 284, 76
Slipher V. M., 1913, Lowell Observatory Bulletin, 2, 56
Soszyński I., Gieren W., Pietrzyński G., Bresolin F., Kudritzki R.-P., Storm J., 2006, ApJ, 648, 375
Springel V., et al., 2005, Nature, 435, 629
Steigman G., Turner M. S., 1985, Nuclear Physics B, 253, 375
Teyssier M., Johnston K. V., Kuhlen M., 2012, MNRAS, 426, 1808
Thompson R., Nagamine K., 2012, MNRAS, 419, 3560
Tisserand P., et al., 2007, A&A, 469, 387
Tucker W. H., Tananbaum H., Remillard R. A., 1995, ApJ, 444, 532
Tully R. B., et al., 2013, AJ, 146, 86
Zhao H., Famaey B., Lüghausen F., Kroupa P., 2013, A&A, 557, L3
van den Bergh S., 1999, ApJL, 517, L97
van der Marel R. P., Fardal M., Besla G., Beaton R. L., Sohn S. T., Anderson J., Brown T., Guhathakurta P., 2012a, ApJ, 753, 8
van der Marel R. P., Besla G., Cox T. J., Sohn S. T., Anderson J., 2012b, ApJ, 753, 9

This paper has been typeset from a TEX/LATEX file prepared by the author.